RADIX / SYSTEMS

Report Number: TR-94-089

Radix Systems, Inc. 50 lb. Moving Magnet Actuator Digital Controller - Design and Implementation

DTIC
SELECTED
SEP 2 6 1995
F

Charles E. Chassaing
Mark J. Jones

Prepared by:

Radix Systems, Inc.
6 Taft Court
Rockville, MD 20850

DISTRIBUTION STATEMENT A
Approved for public release
Distribution Unlimited

October 1994

Contract No. N00014-92-C-0200

Prepared for:

Office of Naval Research
Department of the Navy
800 N. Quincy Street
Arlington, VA 22217-5000
Attn: JAD, Code: 1221

DTIC QUALITY INSPECTED 5

19950922 070

RADIX / SYSTEMS

Report Number: TR-94-089

Radix Systems, Inc. 50 lb. Moving Magnet Actuator Digital Controller - Design and Implementation

Charles E. Chassaing
Mark J. Jones

Accesion For
NTIS CRA&I ☑
DTIC TAB ☐
Unannounced ☐
Justification
By partti
Distribution /
Availability Codes
Dist | Avail and / or Special
A-1

Prepared by:

Radix Systems, Inc.
6 Taft Court
Rockville, MD 20850

October 1994

Contract No. N00014-92-C-0200

Prepared for:

Office of Naval Research
Department of the Navy
800 N. Quincy Street
Arlington, VA 22217-5000
Attn: JAD, Code: 1221

TABLE OF CONTENTS

1.0 INTRODUCTION

This document discusses the development and testing of a digital feedback controller on the Radix Systems, Inc. 50 lbf convectively cooled moving magnet actuator. The shaker design and performance without the digital controller are discussed in detail in Reference 1.

The purposes of the digital controller are twofold: to flatten the shaker lbf/voltage frequency response and to reduce the total harmonic distortion in the 26 to 200 Hz operating band. The controller makes use of the moving mass acceleration and/or the shaker voice coil electrical current feedback signals to reduce the shaker distortion. Radix Systems, Inc. testing of analog feedback control systems on moving coil transducers has shown that reduction in distortion is possible through feedback by increasing the open loop gain of the system at the drive frequency harmonics. A digital controller provides increased flexibility in the choice of compensation for the feedback, and unlike analog compensation which is hardwired, allows for easy changes to the compensation through software. This is especially significant for shakers used in Naval applications because the frequency response of the shaker is dependent upon the impedance of the structure to which it is mounted; therefore, the feedback compensation also has this dependency.

A digital controller also provides the possibility of developing the feedback compensation on-line. With an analog controller, testing must be conducted to determine the shaker frequency response at the mounting location, and then the proper compensation developed off-line (for example, in an office with computing facilities) and hardwired in the laboratory. With a digital controller, the system identification and compensation can be determined on-line without human intervention. A technique and software for implementing such a process, as well as a simulation of the technique on the Radix Systems' 50 lbf shaker is described in this report.

The report is organized into six major sections. The first section discusses the overall control concept, and presents the desired and uncompensated shaker or plant frequency responses. The second section provides a brief discussion of the control system hardware and the low-level software used to operate the hardware. The third section discusses the control system theory and techniques used to develop the digital compensation. Several techniques are described, from a classical transform theory design approach to a direct digital design technique and a modern state space design approach. The fourth section discusses the actual compensation designs for feedback control of the Radix Systems' shaker, and provides the open and closed loop responses for each of the designs. The fifth section provides results of the distortion testing, and discusses the factors that may make one design better than another from a distortion standpoint. Finally, the sixth section discusses a technique and software for implementing the entire digital feedback control process on-line.

This report concludes the work required for the Office of Naval Research Contract N0014-92-C-0200. A total of five formal technical reports have been issued summarizing the technical work under this contract: three reports on the 500 lbf water-cooled prototype shaker (References 2, 3, and 4), one report on the 50 lbf convectively-cooled shaker (Reference 1), and the subject report.

2. CONTROL CONCEPT AND THE DESIRED AND UNCOMPENSATED PLANT FREQUENCY RESPONSES

As described in detail in Reference 1, the Radix Systems, Inc., 50 lbf moving magnet actuator or shaker is a permanent magnet electromagnetic device that develops force when current is passed through coils permanently mounted at right angles to the magnetic field. A cross-sectional sketch of the shaker is shown in Figure 2.1. In response to this force, the moving magnet slides on the shaft and is resisted by coil springs which act to keep the magnet centered in the shaker. The motion of the moving mass is governed by a coupled set of differential equations which can be approximated by the following two equations:

$$M\ddot{x} + C\dot{x} + Kx = BlI$$
$$IR + L\dot{I} + Bl\dot{x} = V$$

V = Drive Voltage
x = Mass Displacement
I = Electric Current

R = Coil Resistance
L = Coil Inductance
M = Moving Mass
K = Spring Stiffness
B = Magnetic Field
l = Wire Length
C = Mechanical Damping

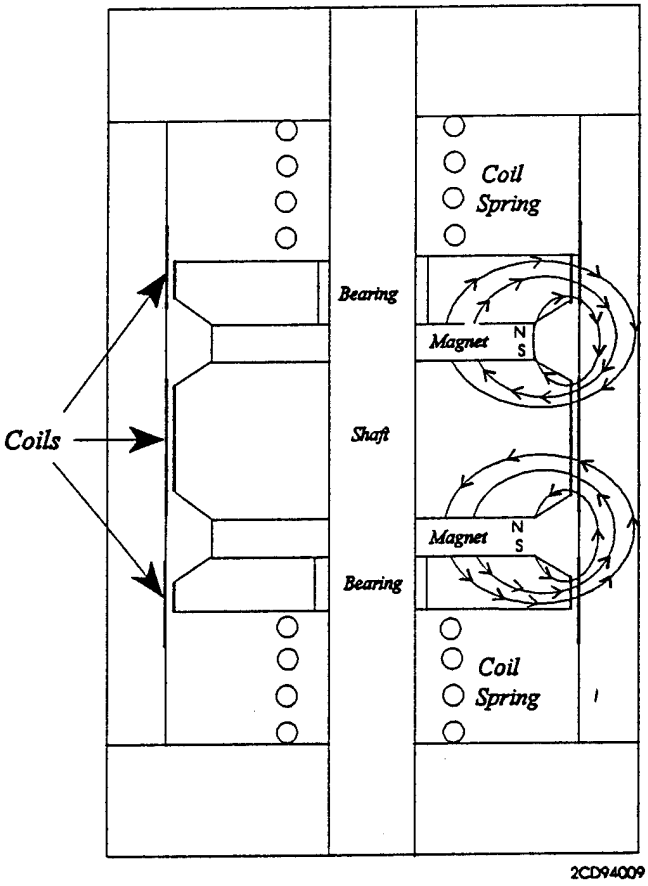

Figure 2.1

The frequency response of the plant as measured is shown in Figure 2.2. In this test and for all testing discussed in this paper, the shaker is mounted vertically on a 3000 lbm block which is isolated from the floor by air tires. The test setup is shown in Figure 2.3. The y-axis of the magnitude plot in Figure 2.2 is given in units of volts/volts. The numerator corresponds to the voltage output of an accelerometer mounted on top of the moving mass. The denominator volts correspond to the source voltage of the signal analyzer used to conduct the test. An amplifier with a gain of 26 dB amplifies the source voltage. The accelerometer has an output of 200 mV/g, and the moving mass has a mass of 6.6 lbm. Based on this, the accelerometer voltage corresponds to 33 lbf/V.

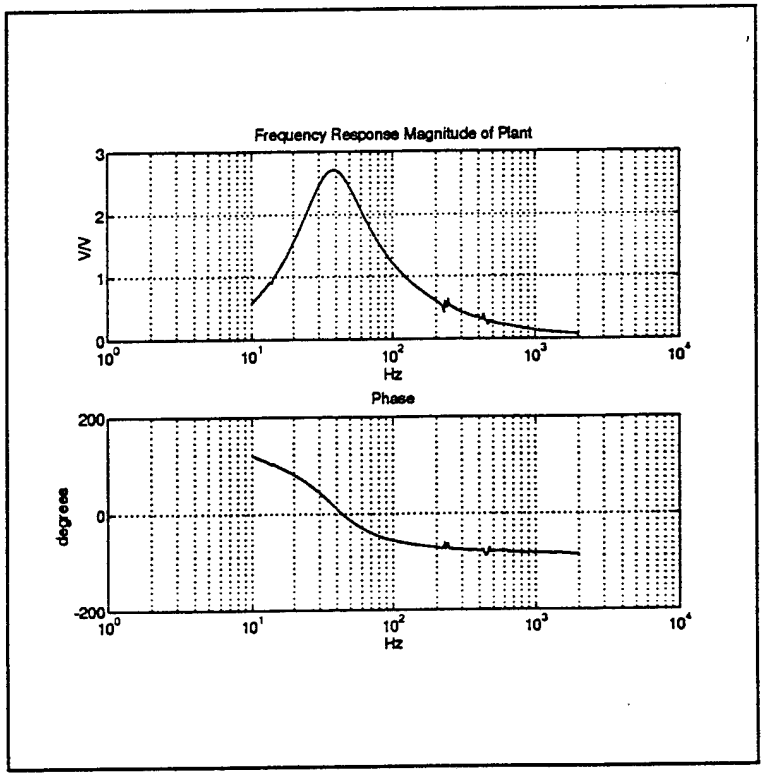

Figure 2.2

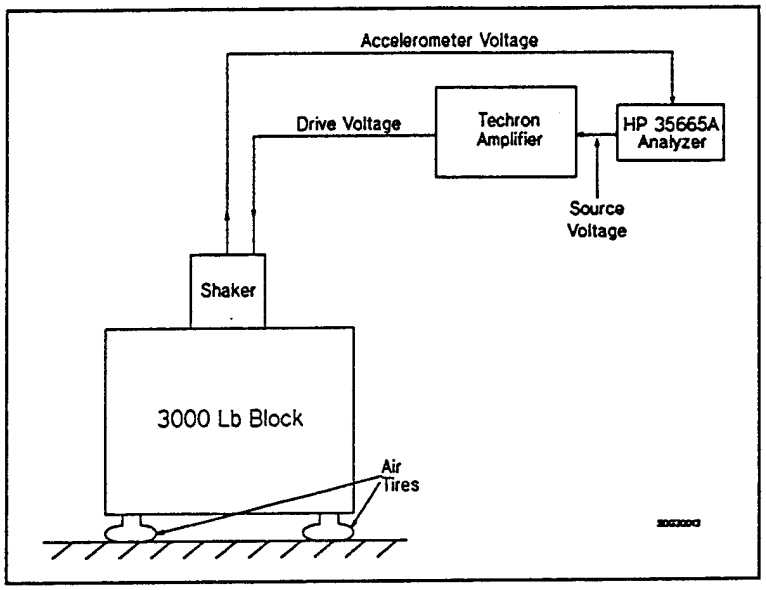

Figure 2.3

The ideal closed loop plant frequency response would be maximally flat in the passband of 26 to 200 Hz and at higher frequencies if possible. A Butterworth passband filter response is maximally flat in the passband and is therefore a good candidate for the desired closed loop plant response. A candidate Butterworth filter desired plant response is shown in Figure 2.4. (Details of the filter design are discussed in Section 5.) The actual breakpoints of the filter will be determined during the compensation design. The magnitude in the passband has been selected to be 1.0 V/V; therefore one source volt in corresponds to one accelerometer volt out or 33 lbf.

Radix Systems, Inc. has found during analog feedback testing of transducers that the total harmonic distortion is related to the amount of open loop gain at the harmonics; the more gain at the harmonics, the less the distortion. Therefore, in addition to providing a flat closed loop response in the operating range, the compensation should provide as much open loop gain as practicable to minimize distortion.

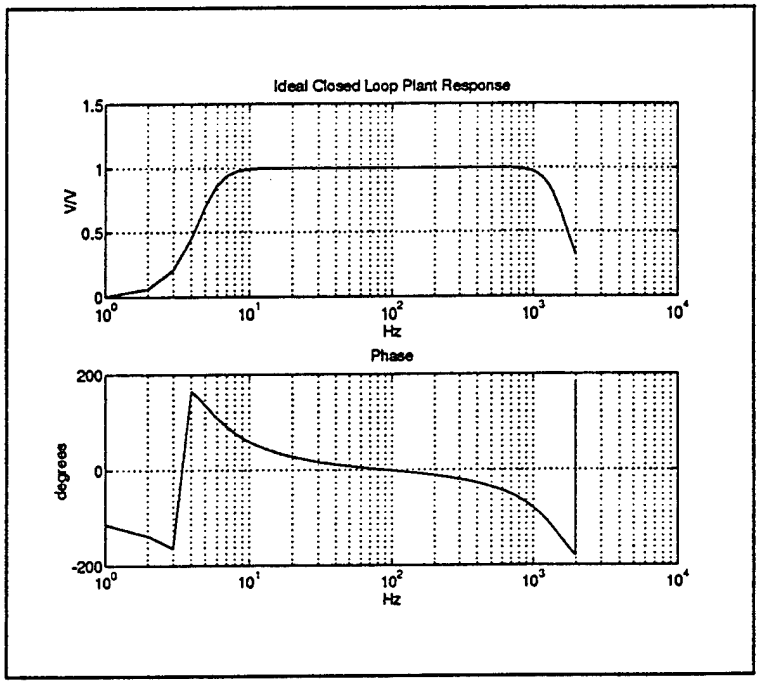

Figure 2.4

The overall control system will have a form similar to that shown in Figure 2.5 below.

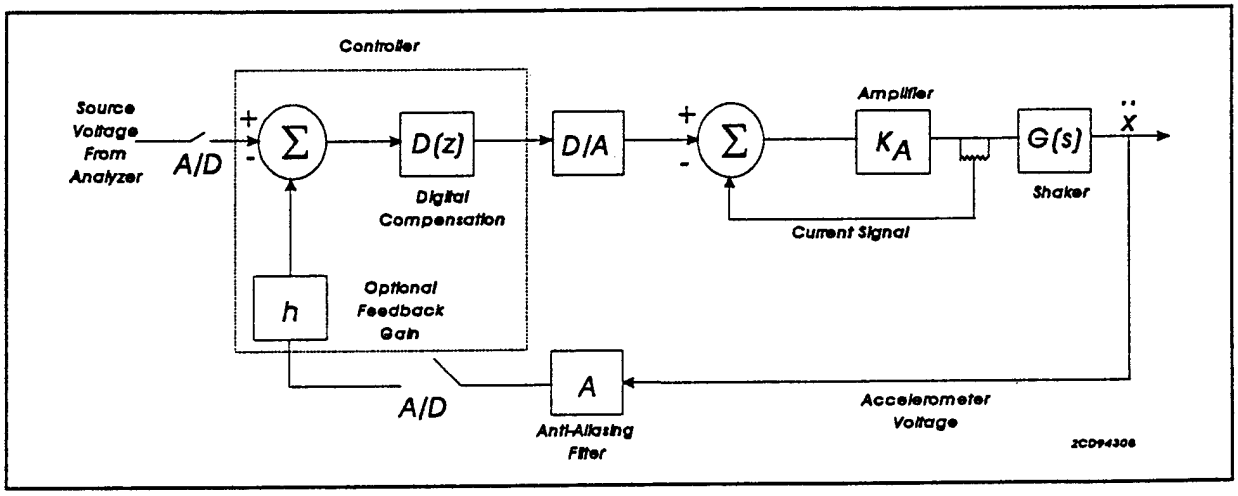

Figure 2.5

The system consists of two analog to digital converters to change the source voltage and feedback voltages to digital signals; a microprocessor and auxiliaries to do the digital filtering of the signals; a digital to analog converter to provide a continuous signal to the amplifier and shaker; and an anti-aliasing filter to prevent high frequency accelerometer noise from interfering with the accelerometer voltage samples. A current feedback loop around the amplifier is also installed. When on, this feedback acts to maintain 10 amps amplifier output per source volt into the amplifier, and the amplifier is considered to be in "constant current mode." The frequency response for the shaker plus amplifier shown in Figure 2.2 is with the amplifier in "voltage mode," i.e., with the current feedback off. The shaker plus amplifier response with the current feedback on will be different than Figure 2.2; hence, different compensation D(z) will be required. Compensation with and without current feedback will be developed.

The design goal, therefore, is to determine the digital filter or compensation D(z) that will produce a closed loop response, or overall system frequency response, that has magnitude of approximately 1.0 in the 26 - 200 Hz passband or as far out in frequency as practicable, and which provides as much open loop gain as practicable in order to minimize the total harmonic distortion. The design of this compensation will be discussed in Sections 4 and 5.

3. CONTROL SYSTEM HARDWARE AND LOW-LEVEL SOFTWARE

Functional requirements of the control system hardware were briefly mentioned in the last section and are well depicted by Figure 2.5. The hardware consists of analog to digital converters, digital to analog converters, a digital signal processing board with microprocessor, an anti-aliasing filter, and associated auxiliary boards to allow communication and coordination between the hardware components. The purpose of this section is to discuss the operation and function of this hardware as it pertains to the control problem. Therefore, issues such as how samples are obtained, the sampling rate, the controller delay, etc., will be investigated. Other issues such as the system memory

mapping, communication protocols between boards, and the detailed low-level "driver" software written by Radix Systems, Inc., to initialize and coordinate the board operation, will not be investigated in depth.

The controller hardware is contained on four separate VME bus boards. Each of the boards connects to a VME backplane which is connected to a 5V DC power supply. The boards - a digital signal processing board; a D/A, A/D board; a MIX bus master baseboard; and an anti-aliasing filter board - are approximately nine inches high, six inches deep, and one inch wide. All of the hardware is contained in a standard subrack.

The digital signal processing board is a Pentek Model 4270 which contains Texas Instruments TMS320C40 microprocessors. The TMS320C40 is a 32-bit floating point processor with a 50-ns cycle time which allows it to execute operations at up to 40 million floating point operations per second. The board contains 8 Mbytes of SRAM. This powerful board was selected because it allows fast sampling rates and has the capability of handling the automated digital compensation design process discussed in Section 7.

The A/D, D/A board contains eight A/D input channels and four D/A output channels, each with 16-bit resolution. All the input and output channels are simultaneously sampled/updated at rates up to 100 kHz/channel. The A/D's each have a separate track-and-hold amplifier and therefore can be modeled as zero-order hold (ZOH) devices during the digital compensation design process. All of the channels have first-in-first-out (FIFO) buffers to prevent loss of data during delays and startup. The sampling clock can be set either internally by dividing down a 12 MHz crystal, or externally via a clock signal to a front panel connector.

The MIX baseboard is a Pentek Model 4201 with 1 Mbyte of SRAM. The function of the board is to control the communication among the other system boards. It also provides an output

to a DEC VT320 monitor. This allows the results of C-code printf statements to be viewed on the monitor during control system operation. The last board contains the anti-aliasing filters. This board was designed with a cut-off frequency of 50 kHz in anticipation of using a system sampling rate of 100 kHz.

A C-compiler and emulator comes with the digital signal processing board and allows the microprocessor instruction set to be written in C-code on a personal computer and down-loaded to the microprocessor. This software also allows for debugging of the C-code and off-line access to the data in system registers and memory locations. Single stepping through the assembly language generated by the compiler is also possible with the debugger.

To implement the controller, Radix Systems, Inc. has chosen to set the sampling rate with the A/D internal clock. This sampling rate must coincide with an interrupt in the processor so the processor is available to process the samples. The synchronization between the processor interrupt and the A/D board clock is implemented by a phase-locked loop that is contained in the low-level software.

When the processor receives an interrupt, it stops what it is doing, places its register data on the stack, and jumps to the sample processing function. The sample processing function contains the digital compensation algorithm. This algorithm must be completed within a sampling interval. After completing the function, the processor retrieves the stack data and continues on as if it were not interrupted.

If the controller does nothing but implement the digital compensation, the processor is essentially idle when it is not processing a sample. However, if the controller is programmed to perform other functions, such as is required by the automated digital compensation process, then the controller can perform those functions "off-line" when it is not processing a sample.

The first tests conducted on the controller established the maximum possible sampling rate. This testing sampled one of the input data channels and passed it to an output data channel with no processing whatsoever. This is the shortest possible control algorithm; therefore, it establishes the maximum sampling rate of the system. Testing showed that the maximum possible sampling rate was approximately 30 kHz. At rates faster than this, the processor could not complete the sample processing function within a sampling interval. This result was somewhat surprising, as it was expected that sampling rates of up to 100 kHz would be easily obtainable. It was determined that a 10 kHz sampling rate would approximately split the time the processor spent in the foreground processing the samples and in the background performing what other functions were required. Because the sample rate will be only 10 kHz, the 50 kHz anti-aliasing filter will not perform its intended function. For this reason, this filter will not be used in the control system. This appears acceptable because the frequency response of the plant is itself a low-pass filter which should eliminate aliased signal components. The only source of aliasing would have to come from the controller or accelerometer noise.

This same testing showed that there was a significant delay in the controller. Figure 3.1 shows the frequency response function for the controller with no control algorithm. The gain in the frequency response function is a result of the fact that full scale voltage on the input A/D is 4.5 volts and full scale voltage on the output D/A is 10.0 volts; hence, the gain is $\frac{10.0}{4.5}$. The slope of the phase curve indicates the delay of the system. Pure delay has a frequency response function given by $e^{-j\omega T}$, where T is the time delay. The phase, in radians, of this function is $-\omega T$; therefore, the slope of the phase curve is $-T$, the time delay of the system. The slope of the phase curve is 0.00035 secs. The sampling rate of the controller during this test was 10 kHz; therefore, there is a 3.5 sample delay. A ZOH introduces a one-half sample delay; hence, there is a 3 sample delay in addition to the ZOH delay.

Further testing with the controller showed that the delay sometimes was 4.5 samples. Once the controller was booted up, the control delay would remain constant at 3.5 or 4.5 samples, but it was not possible to determine beforehand which delay would occur. To ensure that the closed loop system would remain stable with either delay, the digital compensation was designed for a 4.5 sample delay.

This delay - other than the ZOH delay - was completely unexpected and is very troublesome for feedback control. The delay will limit the bandwidth of the feedback controller, and will make the closed loop system design objectives less obtainable.

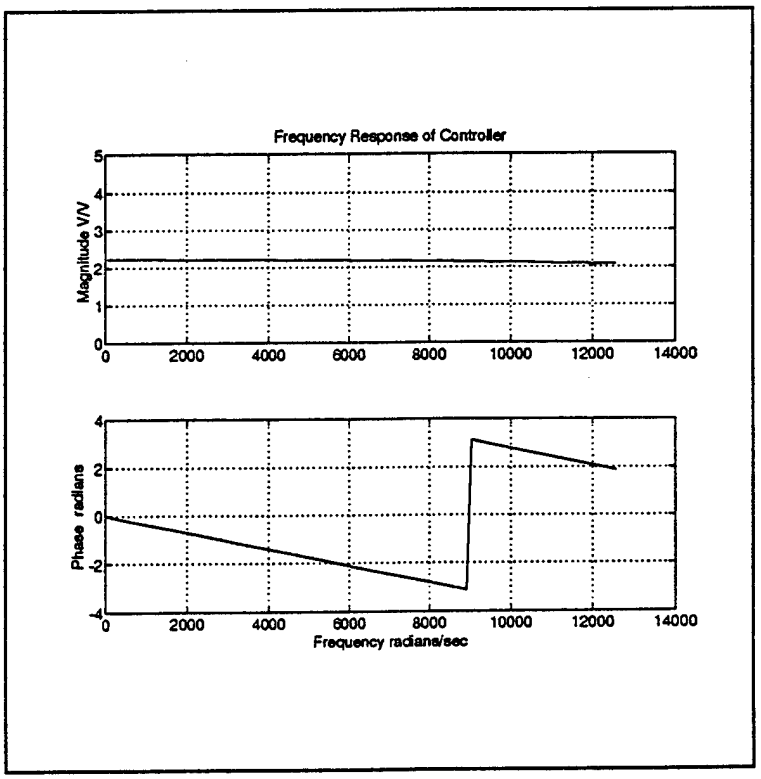

Figure 3.1

4. CONTROL THEORY AND TECHNIQUES

There are a number of different methods of designing digital control systems. Three of these methods, as they pertain to the subject control problem, are discussed in this section: direct digital control, classical control, and modern or state space control. The direct digital control method takes advantage of the fact the realization of digital compensation networks are not constrained by the hardware limitations of resistors and capacitors as in analog design. Therefore, the overall closed loop transfer function, $H(z)$, can be specified and the compensation designed to produce this transfer function.

Classical control or transform methods are fundamentally associated with the mathematical theory of control systems. With these methods, the compensation is designed either by placing the poles of the closed loop system (root-locus methods) or by adjusting the open loop response of the system (frequency response methods).

Modern or state space control methods come from the state variable method of modeling dynamic systems. In this method, dynamic systems are described by a set of first order differential equations called the state. State space control techniques are involved directly with control of the state variables, and normally attempt to place the poles of the state space system at desired locations. The state space method is particularly well suited for multiple-input, multiple-output control.

4.1 Direct Digital Control

The control system for the shaker can be modeled by the system shown in Figure 4.1. The blocks identify z-domain transfer functions; $D(z)$ is the compensation transfer function; $G(z)$ is the plant transfer function. The constant h is a feedback gain that may also contain a delay unit z^{-n}. In direct digital control, the desired transfer function $H(z)$ is given, as is the plant transfer function $G(z)$.

For the moment, assume that the feedback gain h is also given. The goal is to determine the compensation $D(z)$ that produces the desired closed loop transfer function $H(z)$. It is easy to show that $H(z)$ is given by the following transfer function:

$$H(z) = \frac{D(z)\ G(z)}{1 + h\ D(z)\ G(z)} \tag{1}$$

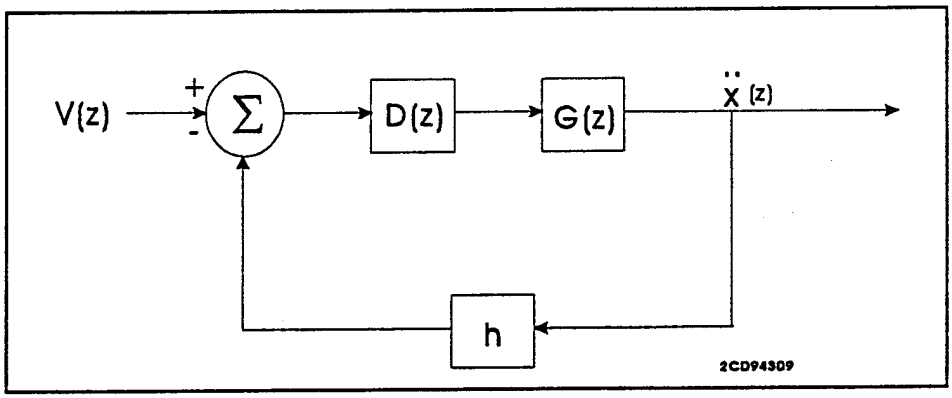

Figure 4.1

This equation can be solved for $D(z)$:

$$D(z) = \frac{H(z)}{G(z)\ (1 - h\ H(z))} \tag{2}$$

From this equation, it can be seen that the compensation must cancel the plant effects and add whatever is necessary to give the desired result. Although this equation will yield a mathematical result for any $G(z)$ and $H(z)$, the result $D(z)$ may not be physically realizable and the overall system may not be stable. This is best understood by splitting the compensation $D(z)$ into two separate transfer functions - $\beta(z)$ and $G^{-1}(z)$ - as shown in Figure 4.2.

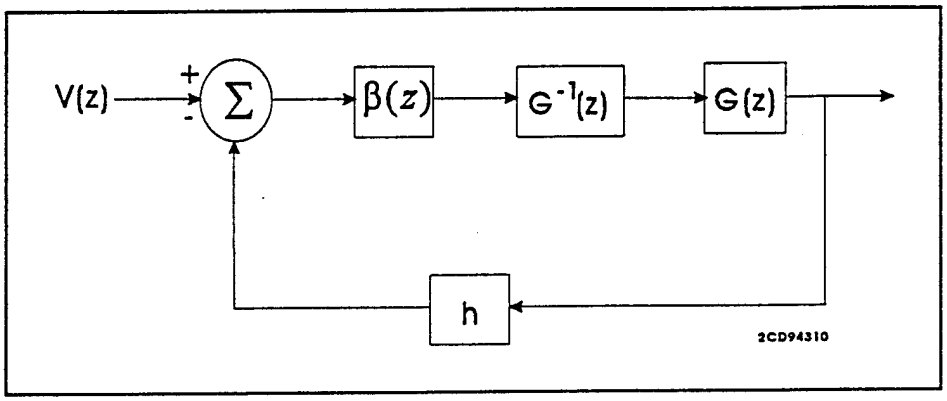

Figure 4.2

$G^{-1}(z)$ is the reciprocal of $G(z)$, such that $G^{-1}(z)\,G(z) = 1$ for all z. It is clear that the roots in the numerator of $G(z)$ (i.e., zeros) are in the denominator of $G^{-1}(z)$ (i.e., poles). If $G(z)$ contains any non-minimum phase zeros (i.e., zeros with magnitude greater than 1), then $G^{-1}(z)$ and the overall system will be unstable. To prevent this situation from occurring, the non-minimum phase zeros must be included as part of the desired plant $H(z)$. When this is done, the denominator of $G^{-1}(z)$ can be modified to include only the minimum phase zeros of $G(z)$; therefore, $G^{-1}(z)$ will be stable.

This process has a physical interpretation in the time domain. A non-minimum phase zero contains some delay; when the zero is at infinity, it is a pure delay (z^{-1}). It is physically impossible to remove the delay in a plant by using compensation. Therefore, the desired transfer function must contain the delay elements in order for it to be physically realizable.

Figure 4.2 simplifies to Figure 4.3 when the desired transfer $H(z)$ is modified to contain the non-minimum phase zeros of $G(z)$. $N(z)$ is a transfer function containing the non-minimum phase zeros of $G(z)$. The desired closed loop transfer function, $H(z)\,N(z)$, is then given by:

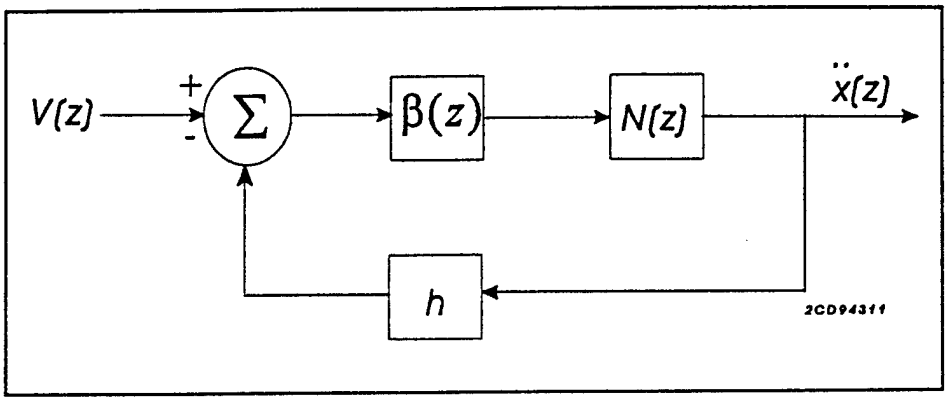

Figure 4.3

$$H(z)N(z) = \frac{\beta(z)N(z)}{1 + h\beta(z)N(z)} \tag{3}$$

and the required compensation $\beta(z)$ is given by:

$$\beta(z) \equiv \frac{H(z)}{1 - hH(z)N(z)} \tag{4}$$

In the compensation design for the shaker, the desired plant $H(z)$ will be a Butterworth bandpass filter. The feedback gain h will be selected so that the maximum open loop gain of the system does not exceed the greater of 40 dB (arbitrarily chosen) or the gain that renders the transfer function $\beta(z)$ unstable.

For the shaker, this will complete the direct digital control design process. The overall compensation $D(z)$ is given by $\beta(z)\ G_{mp}^{-1}(z)$ with feedback gain h, where $G_{mp}^{-1}(z)$ is the reciprocal of $G(z)$ with the non-minimum phase zeros removed. This compensation design process can be performed entirely by the digital controller. The method of automating this process is discussed in Section 7.

4.2 Classical Control

The body of theory associated with classical control is voluminous and is the subject of entire textbooks. This section will touch only on those classical techniques used to develop a digital compensation design for the shaker. The purpose of the investigation is to contrast the performance of this compensation with those developed with the other techniques discussed in this paper.

There are two classical approaches to digital compensation design: (1) perform a continuous design and digitize the resulting compensation, and (2) digitize the plant model and design the compensation in the digital domain. The continuous design method will be chosen for simplicity. This method sometimes results in poor compensation design when the sampling rate is close to the bandwidth of the system. For the shaker, the sampling rate of 10 kHz is greater than ten times the bandwidth; this sampling rate is considered adequate to prevent errors in this application.

The control system for the shaker in the continuous domain can be modeled by the system shown in Figure 4.4. This system is the same as that shown in Figure 4.1 except that the independent complex variable z has been replaced by the complex variable s to indicate the transfer function blocks are LaPlace transforms of continuous rather than discrete time functions. The amplifier, controller, and sensor gains have also been split out from the plant $G(s)$ to aid in the compensation design. The transfer function block identified by Ke^{-sT} includes these gains plus the controller delay T in the system.

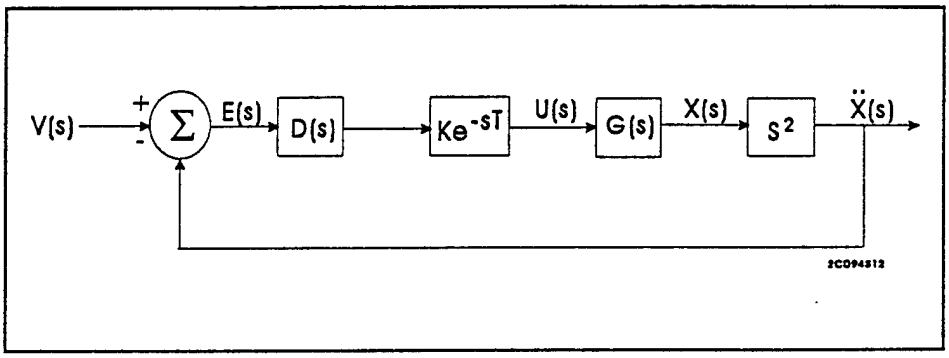

Figure 4.4

The classical design process can be carried out without explicitly defining the plant *G(s)* by working with the open loop frequency response of the system. Simplistically, the open loop gain must be less than 0 dB at all 180 degree phase crossings or the system will be closed loop unstable. Compensation zeros and poles are added to shape the response as desired as long as the stability requirements are maintained. This is essentially the frequency response method of design. The root locus design method requires *G(s)* to be defined explicitly. This method looks at the effects of changes in the feedforward gain on the closed loop poles of the system. This method is a useful way for the designer to understand the effects of compensation on the closed loop poles of the system.

For the shaker, the function *G(s)* will be defined because it is fairly straightforward and reasonably accurate to do so. As stated in Section 2, the equations governing the physics of the shaker are:

$$M\ddot{x} + C\dot{x} + Kx = BlI$$
$$IR + L\dot{I} + Bl\dot{x} = V$$

V = Drive Voltage
x = Mass Displacement
I = Electric Current

R = Coil Resistance
L = Coil Inductance
M = Moving Mass
K = Spring Stiffness
B = Magnetic Field
l = Wire Length
C = Mechanical Damping

To solve for $G(s) = \frac{X(s)}{U(s)}$, take the LaPlace transforms of each of these equations and eliminate $I(s)$:

$$G(s) = \frac{X(s)}{U(s)} = \frac{B\ell}{ML\,s^3 + (MR + CL)s^2 + (CR + KL + B\ell^2)\,s + KR} \tag{5}$$

The overall open loop transfer function of the system is given by:

$$G_0(s) = K\,e^{-sT}\,G(s)\,s^2 \tag{6}$$

$G_0(j\omega)$ should provide a reasonable fit to the measured frequency response function. The delay term e^{-sT} is a non-rational function; therefore, Equation (6) is not a polynomial function. To aid in the root-locus evaluation of the system, e^{-sT} can be replaced by the Pade[1] approximate:

$$e^{-sT} \cong \frac{1 - \frac{sT}{2} + \frac{s^2T^2}{10} - \frac{s^3T^3}{120}}{1 + \frac{sT}{2} + \frac{s^2T^2}{10} + \frac{s^3T^3}{120}} \tag{7}$$

With this substitution, $G_0(s)$ is approximated by a polynomial function and the root-locus of the system can be determined.

The compensation $D(s)$ in classical design is normally a combination of three different types of feedback units: proportional, derivative, and integral. Proportional feedback is linearly proportional to the error signal $E(s)$ (see Figure 4.4) and is therefore a simple gain. Derivative feedback and integral feedback as their names imply are related to the derivatives and integrals of the error signal and have the forms $s + a$ and $\frac{1}{s+b}$ respectively, where a and b are constants. For the

---

[1]Franklin, Gene, "Feedback Control of Dynamic Systems," pp 209-210, Addison Wesley, 1991.

shaker, a combination of these three types of units will be investigated in a compensation design known as a lead or lag compensator:

$$D(s) = K \frac{Qs + 1}{\alpha Qs + 1} \tag{8}$$

where K, Q, and α are constants that are determined by the designer. The design is a lead compensator when $\alpha < 1$ because this compensation results in an open loop phase increase; when $\alpha > 1$ the system design is a lag compensator because it results in an open loop phase decrease. Further details of this compensation design process will be discussed in the next section when the actual compensation for the shaker is designed.

Once $D(s)$ is obtained, it must be transformed into the discrete domain for implementation in the digital controller. The bilinear transform has been chosen to perform this transformation. The bilinear transform maps the entire left-half plane of the s-domain into the unit circle of the z-domain and therefore ensures that stable systems are mapped into stable systems. It works well when the sampling rate is much greater than the bandwidth of the system as in the shaker application. The bilinear transform is given by the following mapping:

$$s = \frac{2}{T} \frac{z - 1}{z + 1} \tag{9}$$

where T is the sampling period.

4.3 State Space Design

State space design techniques as they apply to the shaker control system have also been examined to develop further insights into the control problem. As with the classical design approach, the body of theory associated with this technique is extensive, and only those aspects applicable to the subject control problem will be reviewed.

The state space design technique begins with the governing equations of motion for the shaker system:

$$\begin{aligned} M\ddot{x} + C\dot{x} + Kx &= Bli \\ L\dot{i} + Ri + Bl\dot{x} &= V \end{aligned} \tag{10}$$

In state space design, this system must be broken down into a set of first order differential equations. Because the current i and the acceleration $\ddot{x}$ can be sensed in the shaker problem, it is prudent to allow these two variables to be part of the state of the system. In the existing form of the differential equations, i is already a state of the system but $\ddot{x}$ is not. To make $\ddot{x}$ a state, differentiate the first equation to get:

$$M\dddot{x} + C\ddot{x} + K\dot{x} = Bl\dot{i} \tag{11}$$

and identify the following states $x_1 = \ddot{x}$, $x_2 = \dot{x}$ and $x_3 = i$. Substitute the states into the revised set of differential equations to get:

$$\begin{aligned} M\dot{x}_1 + Cx_1 + Kx_2 &= Bl\dot{x}_3 \\ L\dot{x}_3 + Rx_3 + Bl x_2 &= V \\ \dot{x}_2 &= x_1 \end{aligned} \tag{12}$$

These equations can be rearranged and placed in the following state space matrix form:

$$\begin{bmatrix} \dot{x}_1 \\ \dot{x}_2 \\ \dot{x}_3 \end{bmatrix} = \begin{bmatrix} \frac{-C}{M} & -\left(\frac{K}{M} + \frac{Bl^2}{ML}\right) & -\frac{BlR}{ML} \\ 1 & 0 & 0 \\ 0 & \frac{-Bl}{L} & \frac{-R}{L} \end{bmatrix} \begin{bmatrix} x_1 \\ x_2 \\ x_3 \end{bmatrix} + \begin{bmatrix} \frac{Bl}{ML} \\ 0 \\ \frac{1}{L} \end{bmatrix} V \tag{13}$$

$$\dot{\underline{x}} = \underline{F}\,\underline{x} + \underline{G}\,u$$

This is the continuous state space representation of the shaker. In order to design the discrete compensation, this system must be discretized. It has been shown in many textbooks on this subject that the discrete representation of a continuous state space system subject to ZOH D/A conversion is given by:

$$\begin{aligned} \underline{x}[k+1] &= \underline{\Phi}\,\underline{x}[k] + \underline{\Gamma} u(k) \\ \underline{\Phi} &= e^{\underline{E}T} = \left[\underline{I} + \underline{E}T + \frac{\underline{E}^2T^2}{2!} + \frac{\underline{E}^3T^3}{3!}\cdots\right] \\ \underline{\Gamma} &= \left[\underline{I} + \frac{\underline{E}T^2}{2!} + \frac{\underline{E}^3T^3}{3!}\cdots\right]\underline{G} \end{aligned} \tag{14}$$

In this discrete representation of the state, $\underline{\Phi}$ is the system or transition matrix, *u[k]* is the control input at sample *k*, and *x[k]* and *x[k + 1]* are the state vectors at samples *k* and *k + 1*.

Before proceeding with the feedback analysis, the system must be revised to recognize that there is a delay in the controller. This delay can be incorporated into the discrete state-space representation of the system:

$$\underline{x}[k+1] = \underline{\Phi}\,\underline{x}[k] + \underline{\Gamma}\, u[k-n] \tag{15}$$

where *n* represents an integer amount of sample delay. Equation (15) is not in desirable state space form; to place this in a more convenient form, the sample delay *n* must be removed from the control input *u[k]* and incorporated into the $\underline{\Phi}$ and $\underline{\Gamma}$ matrices. This is done by introducing additional states which represent the delayed inputs. In the shaker problem, the sample delay *n*=4, and the additional states are $x_4 = u[k-4]$, $x_5 = u[k-3]$, $x_6 = u[k-2]$, and $x_7 = u[k-1]$. The revised state space system with these additional states included is:

$$\begin{bmatrix} \underline{x}[k+1] \\ x_4[k+1] \\ x_5[k+1] \\ x_6[k+1] \\ x_7[k+1] \end{bmatrix} = \begin{bmatrix} \underline{\Phi} & \underline{\Gamma} & 0 & 0 & 0 \\ 0 & 0 & 1 & 0 & 0 \\ 0 & 0 & 0 & 1 & 0 \\ 0 & 0 & 0 & 0 & 1 \\ 0 & 0 & 0 & 0 & 0 \end{bmatrix} \begin{bmatrix} \underline{x}[k] \\ x_4[k] \\ x_5[k] \\ x_6[k] \\ x_7[k] \end{bmatrix} + \begin{bmatrix} \underline{0} \\ 0 \\ 0 \\ 0 \\ 1 \end{bmatrix} u[k] \tag{16}$$

$$\underline{x}_D[k+1] = \underline{\Phi}_D \, \underline{x}_D[k] + \underline{\Gamma}_D \, u[k]$$

where $\underline{x}_D$, $\underline{\Phi}_D$, and $\underline{\Gamma}_D$ represent the revised state vectors and matrices. In all further derivations, these delayed versions of the state matrices and vectors will be used; hence, for convenience, the subscript D will be dropped and $\underline{\Phi}$, $\underline{\Gamma}$ and $\underline{x}$ will refer to the delayed versions of the state.

The state space formulation also contains an output equation which defines the outputs which are available from system sensors. For the shaker control problem, the acceleration x_1, and the current x_3 are possible system outputs. For simplicity, the assumption will be made that only one of these sensor signals will be available. This means the output, $y[k]$, is a scalar and can be given by:

$$y[k] = \underline{H} \, \underline{x}[k] \tag{17}$$

where $\underline{H}$ is a 7 x 1 row vector. Equations (16) and (17) makeup the discrete state space representation of the plant.

The plant transfer function $G(z) = Y(z)/U(z)$ is determined by taking the z-transforms of Equations (16) and (17) and solving for $Y(z)$:

$$\frac{Y(z)}{U(z)} = \underline{H} \left[z \, \underline{I} - \underline{\Phi} \right]^{-1} \underline{\Gamma} \tag{18}$$

It is very easy to show that the poles of this system occur when $\det [z \underline{I} - \underline{\Phi}] = 0$. The solution to this equation will result in the eigenvalues of the system matrix $\underline{\Phi}$; therefore, the eigenvalues of $\underline{\Phi}$ are the poles of the transfer function.

At this point, the control input *u[k]* is the uncompensated input source voltage to the shaker, i.e., the samples of the input source voltage from the analyzer. In order to control the dynamics of this system, feedback must be provided. The poles of a state space system can be moved to desired locations by linear state-variable feedback:

$$u[k] = -\underline{K}\, \underline{x}[k] \tag{19}$$

where $\underline{K}$ is a row vector of gains.

The effect of this feedback is to revise the system matrix from $\underline{\Phi}$ to $\underline{\Phi} - \underline{\Gamma}\, \underline{K}$. With a controllable system, a gain vector $\underline{K}$ can be determined to place the system poles in any desired position. With feedback, the system poles are the eigenvalues of $\underline{\Phi} - \underline{\Gamma}\, \underline{K}$.

The use of full state feedback as described in Equation (19) assumes that the full state is available. It has already been stated that only one of the three primary states of the system - acceleration, velocity, current - will be sensed in the shaker problem; therefore, a system has to be devised to estimate the "unsensed" states of the system if full state feedback is used. A procedure for doing this has been devised in state space theory; the control system transfer function which creates the estimated states is called an estimator.

The estimated state, $\hat{\underline{x}}[k]$, is generated by a state space model of the system dynamics and uses the available system information - namely, the control input *u[k]* and the system output *y[k]* - to progressively converge on the true state $\underline{x}[k]$. The estimator equations are given by:

$$\hat{\underline{x}}[k+1] = \underline{\Phi}\,\hat{\underline{x}}[k] + \underline{\Gamma}\,u[k] + \underline{L}\,[y[k] - \hat{y}[k]]$$
$$\hat{y}[k] = \underline{H}\,\hat{\underline{x}}[k] \qquad (20)$$

Notice that these equations are identical to those which model the plant dynamics, with the exception of the new term $\underline{L}[y[k] - \hat{y}[k]]$. This new term - which consists of the estimator gain column vector $\underline{L}$, the output $y[k]$, and the estimated output $\hat{y}[k]$ - serves the purpose of making the estimator dynamics faster than the plant dynamics. This ensures that the estimator error, $\tilde{\underline{x}}[k] = \underline{x}[k] - \hat{\underline{x}}[k]$, converges to zero faster than the plant reaches steady state. It can be shown that the estimator dynamics or poles are given by:

$$\det\ [z\,\underline{I} - [\underline{\Phi} - \underline{L}\,\underline{H}]] = 0 \qquad (21)$$

As long as the system is observable - and the shaker system is both observable and controllable - a gain vector $\underline{L}$ can be determined to place the estimator poles in any desired location.

It is important not to lose sight of the fact that the purpose of the estimator is only to generate the estimated state $\hat{x}[k]$ so that full-state feedback, $u[k] = -\underline{K}\,\hat{x}[k]$, can be employed. With full state feedback, the plant poles are the eigenvalues of $\underline{\Phi} - \underline{\Gamma}\,\underline{K}$ and the estimator poles are the eigenvalues of $\underline{\Phi} - \underline{L}\,\underline{H}$. It turns out that the overall system poles are just a combination of the plant and estimator poles.

The state space control system described thus far has the form shown in Figure 4.5. The control input in this system, $u[k] = -\underline{K}\,\hat{x}[k]$, is not complete because it does not recognize the source voltage from the analyzer $v[k]$. We have had to set this voltage equal to zero in Figure 4.5 to satisfy the system equations discussed thus far. It must be understood that the external input $v[k]$ has no effect whatsoever on the system poles. It does, however, have an effect on the system zeros and hence, the overall transfer function $Y(z)/V(z)$, of the system.

There are many techniques for compensating *v[k]*; the choice of compensation is dependent upon the particular system requirements. In many cases, the compensation of *v[k]* is chosen so that control input *u[k]* to the plant is identical to the control input to the estimator. In the shaker control problem, however, it is desirous for the compensation to work on the error signal, $e[k] = v[k] - y[k]$, because this is the compensation method used in both the classical and direct digital method, and will allow direct comparison between the methods. With this method, the compensation is in the feedforward path and the control input to the estimator is not the same as the control input to the plant. The control equation of the estimator must be revised to include an additional term that acts on the source voltage:

$$\hat{\underline{x}}[k+1] = \underline{\Phi}\ \hat{\underline{x}}[k] + \underline{\Gamma}\, u[k] + \underline{L}[y[k] - \hat{y}[k]] + \underline{M}\, v[k] \tag{22}$$

where $\underline{M}$ is a column vector of gains. Let *u[k]*, the control input to the plant, still remain equal to the full state feedback $-\underline{K}\,\hat{\underline{x}}[k]$, substitute $\hat{y}[k]$ with $\underline{H}\,\hat{x}[k]$, set $\underline{M}$ equal to $-\underline{L}$, and plug into the above equation:

$$\begin{aligned} \hat{\underline{x}}[k+1] &= [\underline{\Phi} - \underline{\Gamma}\,\underline{K} - \underline{L}\,\underline{H}]\,\hat{\underline{x}}[k] + \underline{L}[y[k] - v[k]] \\ u[k] &= \underline{K}\,\hat{x}[k] \end{aligned} \tag{23}$$

By setting $\underline{M} = -\underline{L}$, the compensation is placed in the feedforward path and acts on the difference between the output *y[k]* and the input *v[k]*. The overall system now recognizes and includes compensation for *v[k]*, and simplifies Figure 4.5 into the final result shown in Figure 4.6.

The system shown in Figure 4.6 has the same form as the control systems developed using classical and direct digital control methods. The controller transfer function in the shaker state space application is given by:

$$D(z) = \underline{K}\,[z\,\underline{I} - \underline{\Phi} + \underline{\Gamma}\,\underline{K} + \underline{L}\,\underline{H}]^{-1}\,\underline{L} \tag{24}$$

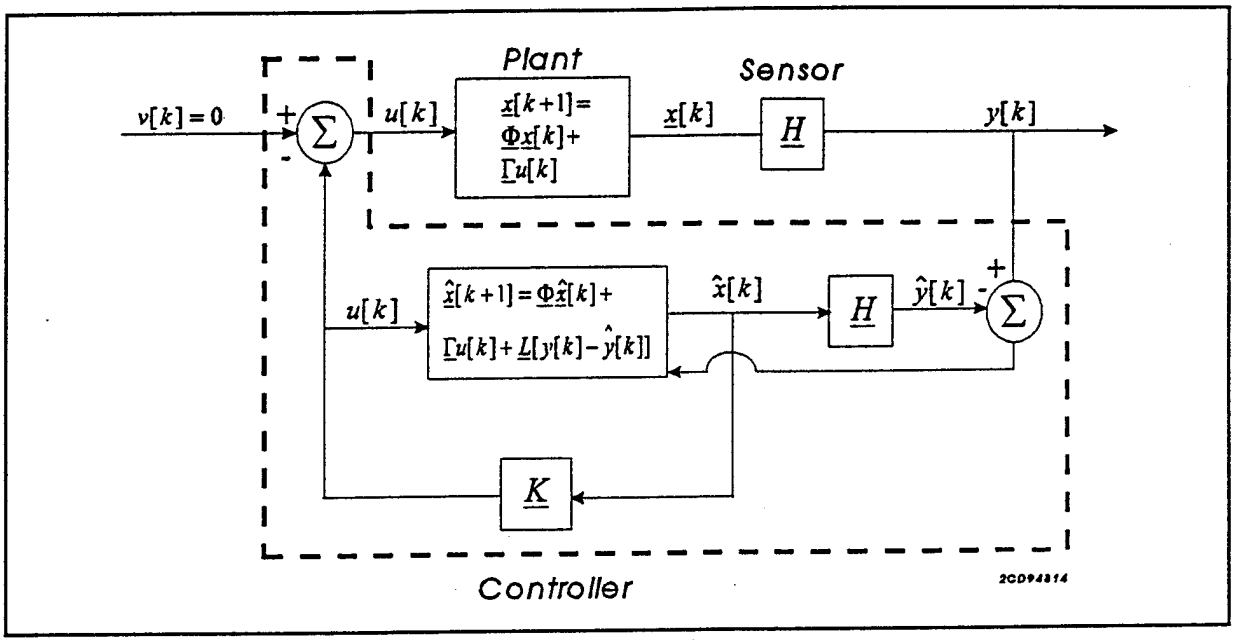

Figure 4.5.

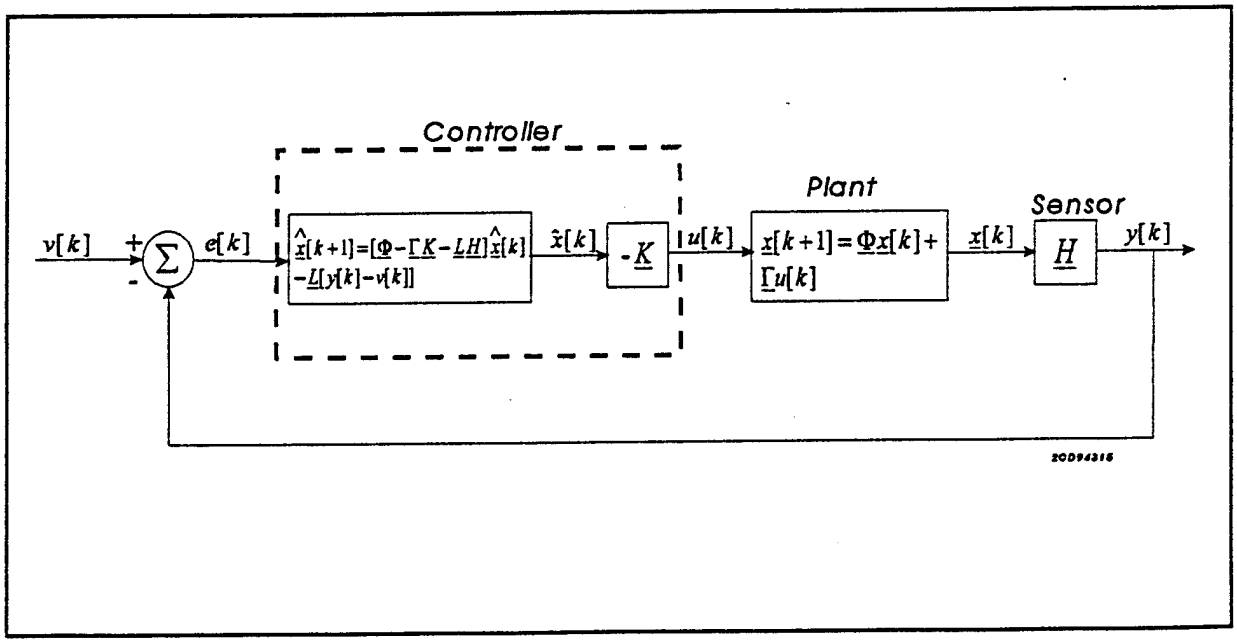

Figure 4.6

and the plant transfer function is given by:

$$G(z) = \underline{H}[z\ \underline{I} - \underline{\Phi}]^{-1}\ \underline{\Gamma} \tag{25}$$

By making these substitutions for the controller and plant/sensor in Figure 4.6, the diagram reverts to the same exact form used for the classical control analysis shown in Figure 4.1.

In summary, the state space design method for the shaker proceeds as follows: (1) determine the system matrices $\underline{\Phi}$, $\underline{\Gamma}$ and $\underline{H}$ from the governing differential equations and the system outputs; (2) select the desired poles for the system and determine the feedback gain vector $\underline{K}$ by recognizing the poles are the eigenvalues of $\underline{\Phi} - \underline{\Gamma}\ \underline{K}$; (3) select faster poles for the estimator and determine the estimator gain vector $\underline{L}$ by recognizing the estimator poles are the eigenvalues of $\underline{\Phi} - \underline{L}\ \underline{H}$; (4) incorporate the time-domain control equations contained in Equation (23) into the controller.

5. SHAKER COMPENSATION DESIGNS

This section discusses the actual compensation designs for the shaker using the techniques discussed in the last section. The predicted and actual open and closed loop responses for each of the design techniques are presented.

5.1 Direct Digital Control Compensation

The voltage controlled frequency response of the shaker plus amplifier is shown in Figure 2.2. To design the compensation for this system, it was found effective to include the control gain and delay in the actual transfer function. This was done by determining the frequency response of the controller/amplifier/shaker with a control algorithm that simply passed the input sample to the output D/A. This combination of the controller/amplifier/shaker will be referred to as the plant. The frequency response of the plant is shown in Figure 5.1.

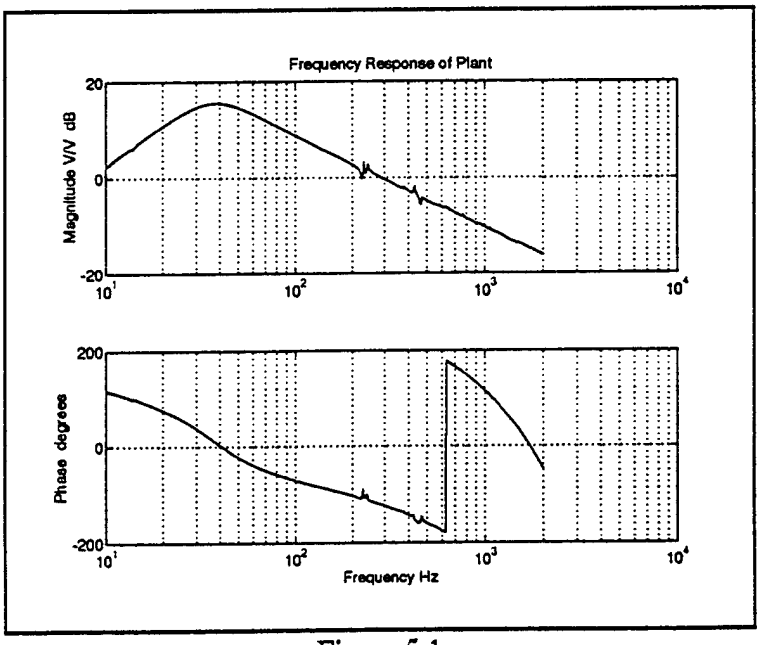

Figure 5.1

The first step in the direct digital control design process is to fit the plant to a *z*-domain transfer function or infinite-impulse response (IIR) filter *G(z)*. The numerical computation software MATLAB was used to perform the curve fit; an 8th-order system was determined to provide an acceptable fit. The curve fit is shown in Figure 5.2.

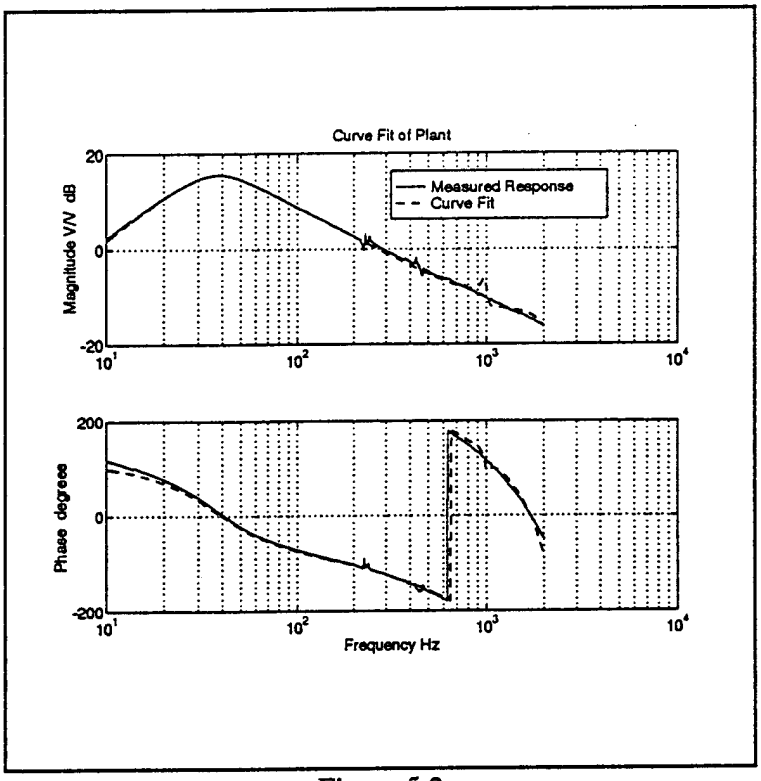

Figure 5.2

The next step is to remove the non-minimum phase zeros from *G(z)*, and include these zeros in the desired plant *H(z)*. The desired plant *H(z)* is a sixth order Butterworth bandpass filter with break points at 5 and 1500 Hz. *G(z)* was found to have four non-minimum phase zeros. The desired plant frequency response $H(e^{j\omega t})$, as well as the modified desired plant response which includes the non-minimum phase zeros, are shown in Figure 5.3. This result shows that only the frequency response phase is significantly affected by the non-minimum phase zeros. The phase curve is affected because the non-minimum phase zeros add delay, in this case the amount of delay associated with the

plant. In other simulations, it was found that non-minimum phase zeros near the unit circle can also greatly affect the desired magnitude response. Fortunately, the non-minimum phase zeros are far enough removed from the unit circle for this not to occur in the shaker control problem.

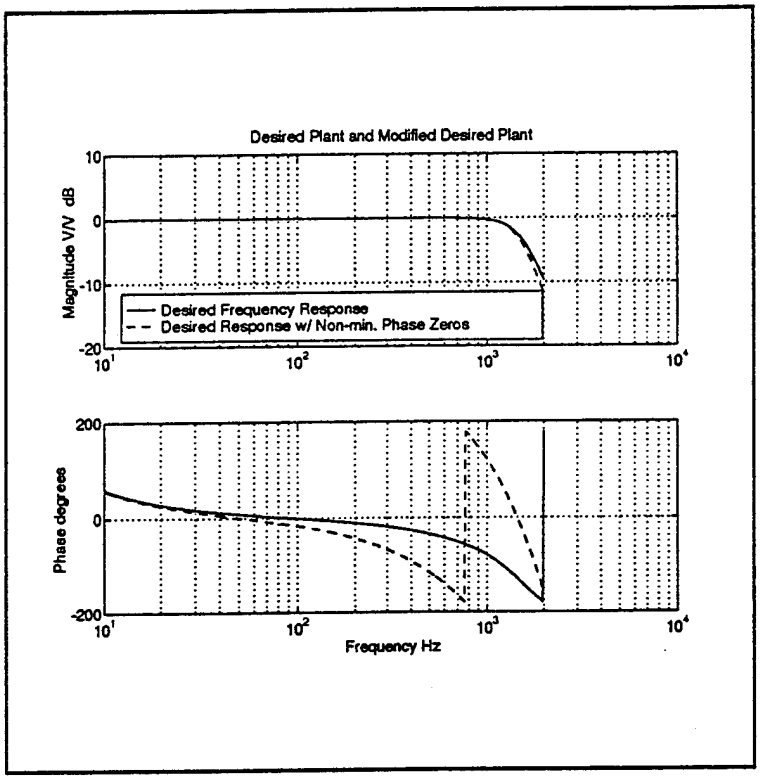

Figure 5.3

The overall control system for the direct digital control method is shown in Figure 5.4. $G_{mp}^{-1}(z)$ has just been determined; to complete the compensation design, $\beta(z)$ and the feedback gain h must be determined. There is no added delay in the feedback path because $\ddot{x}$ and v are sampled simultaneously; therefore, h is a scalar gain. The feedback gain has been selected so that the maximum open loop gain does not exceed 100 or 40 dB. The maximum open loop gain is approximated by 1.0/(1.0 - h); therefore, h was selected to be 0.99. The required compensation $\beta(z)$ can then be determined from the following equation derived in Section 4.1:

$$\beta(z) = \frac{H(z)}{1 - H(z)\, G_{mp}^{-1}(z)\, G(z)} \tag{26}$$

$\beta(z)$ should be checked for stability. If it is unstable, the feedback gain h should be decreased until stability results. $\beta(z)$ for this system was stable at $h = 0.99$. The final compensation is $\beta(z)\, G_{mp}^{-1}(z)$ with feedback gain h.

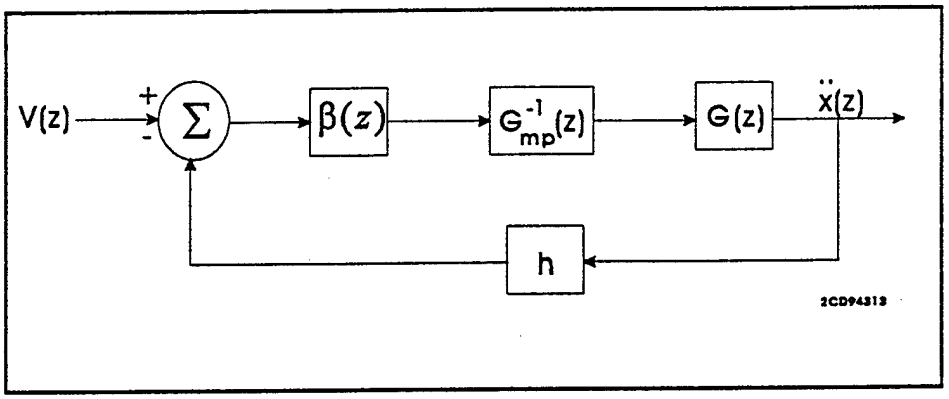

Figure 5.4

The predicted versus actual open loop frequency response for this system is shown in Figure 5.5. These responses match reasonably well. Notice that the maximum open loop gain is about 40 dB as predicted and occurs between 45 and 50 Hz. The frequency of this peak is given by the breakpoints of the Butterworth filter: $f_c = \sqrt{f_1 f_2}$. In this system, the breakpoints are 5 and 1500 Hz so the peak frequency should be about 87 Hz. The peak does not occur at 87 Hz because the non-minimum phase zeros have affected the applicability of this equation. Another ramification of the non-minimum phase zeros is the magnitude peak that occurs at approximately 1200 Hz; in a system with only minimum phase delay, this peak would not exist. The system is just marginally stable at frequencies near this peak.

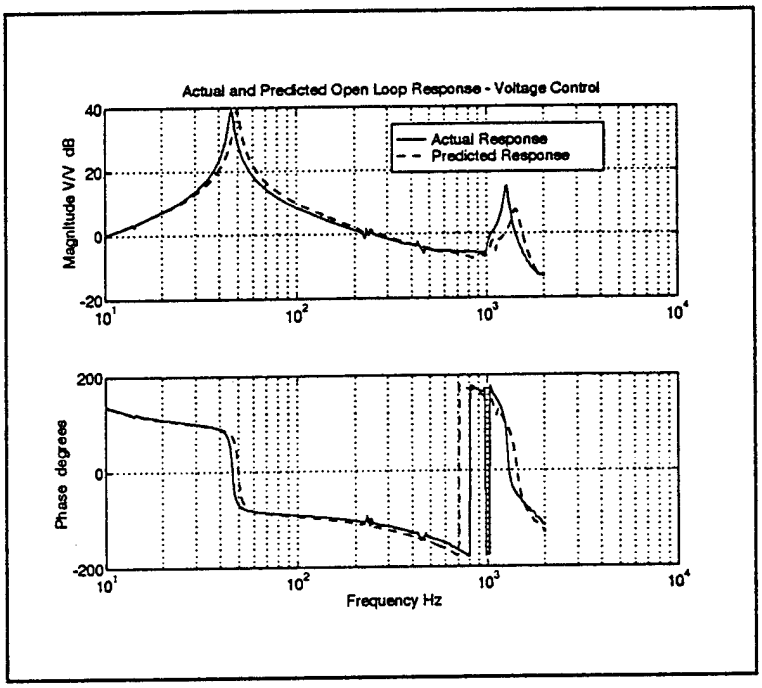

Figure 5.5

The actual and predicted closed loop responses for this system are shown in Figure 5.6. The actual and predicted responses have good agreement with exception of the spike in the actual response at about 1000 Hz. The cause of this spike is most likely related to the fact that the compensation was designed for a controller delay of 4.5 samples and for this particular test the actual controller delay appears to be 3.5 samples.

At this point, a few comments on whether this compensation will meet the stated goals are appropriate. The goals of the compensation are to produce a flat, 0 dB response in the 26 - 200 Hz operating band, and to increase the open loop gain as this should reduce total harmonic distortion. The closed loop response monotonically decreases from about 1.0 to -1.0 dB in the operating range. The response remains reasonably flat (between 0 and -3 dB) out to approximately 900 Hz. The uncompensated plant varies from about 3 to 16 dB in the operating range, and decreases linearly with frequency to about -10 dB at 900 Hz. The compensation appears to have satisfactorily met the

requirement to produce a 0 dB flat response in the operating range. It has increased the bandwidth of the shaker to about 900 Hz. This compensation could be "fine-tuned" to produce a slightly more flat response, and perhaps to eliminate the 1000 Hz spike; however, further changes were considered to produce only marginal improvement and were not implemented.

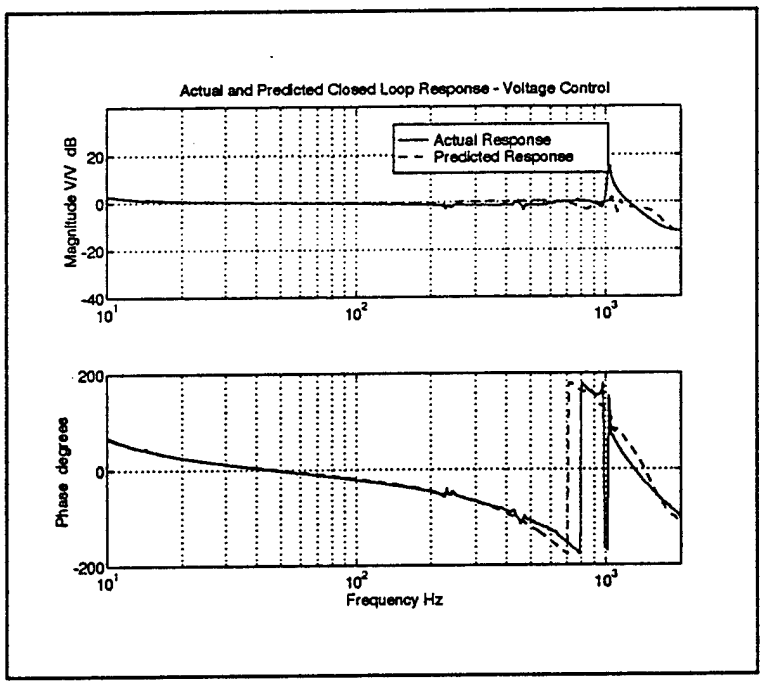

Figure 5.6

The other design goal is increased open loop gain. As expected, the open loop has a maximum gain of 40 dB. With the Butterworth filter design, however, the gain decreases rapidly after the peak. In this case, the gain has decreased to 0 dB at about 200 Hz; therefore, reduction of system harmonics at frequencies greater than 200 Hz cannot be expected. This topic will be discussed in greater detail in Section 6, "Distortion Testing."

A compensation design was also developed using the direct digital control method with the amplifier in current control. As discussed earlier, the amplifier is in current control when a current

feedback loop around the amplifier is turned on. In current control mode, the system will therefore have an inner current feedback loop, as well as an outer acceleration feedback loop. The frequency response of the plant in current mode, as well as the curve fit of the plant, are shown in Figure 5.7. As with the voltage controlled method, an 8th-order IIR filter *G(z)* produced a good curve fit. *G(z)* contains four non-minimum phase zeros. The four non-minimum phase zeros were included in the desired plant *H(z)*.

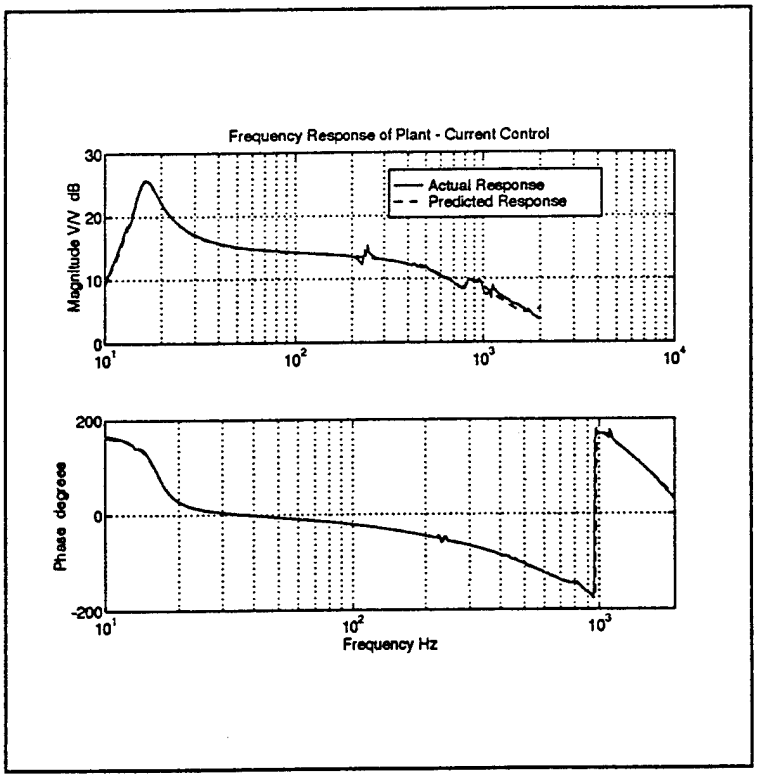

Figure 5.7

As with the voltage response design, the desired Butterworth bandpass response with and without the non-minimum phase zeros differed significantly only in the phase. The predicted and actual open loop and closed loop responses for the system are shown in Figures 5.8 and 5.9, respectively.

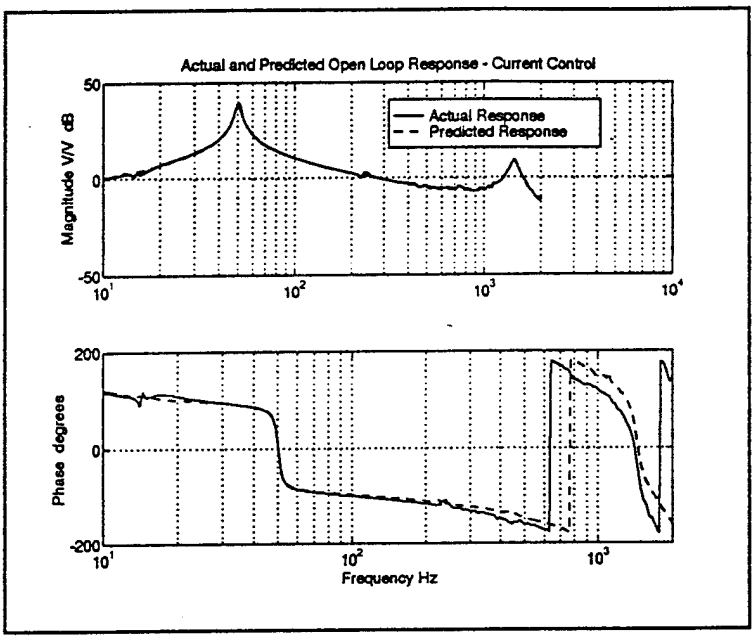

Figure 5.8

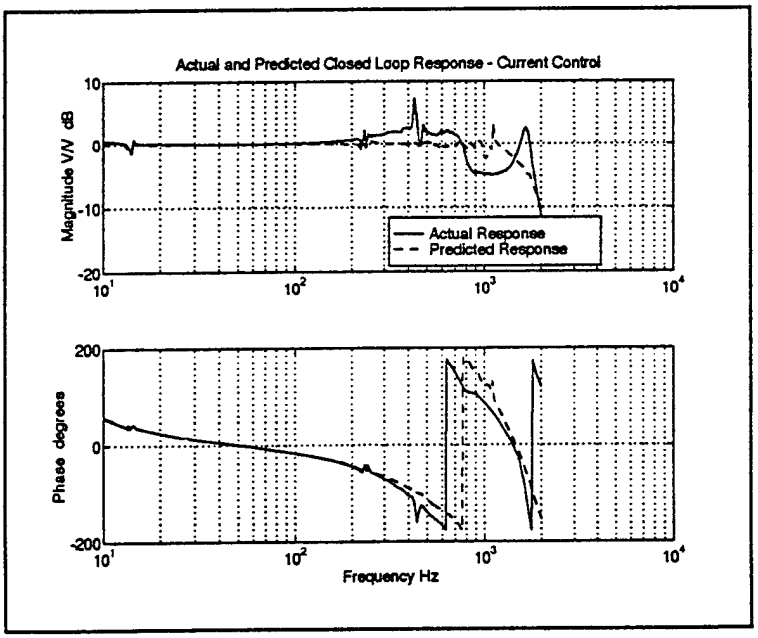

Figure 5.9

The agreement between the predicted and actual responses is reasonable, but is significantly different in the 600 to 2000 Hz range. These differences are probably due to compensation that was designed for 4.5 samples delay and a system that had only 3.5 samples delay during this particular test.

As with the voltage controlled design, the closed loop frequency response is reasonably flat in the 26 to 200 Hz range. The response is essentially 0 dB from 26 to 120 Hz, and increases slightly from there to a little less than 1 dB at 200 Hz. The open loop gain is essentially the same as the voltage controlled design.

5.2 Classical Control Compensation Design

The main reason for examining a classically controlled design is to attempt to increase the open loop gain by more than that obtained by the direct digital control design. The open loop gain with the direct digital control design method decreases to 0 dB by 200 Hz. This is undesirable, because harmonics greater than 200 Hz will not be reduced by feedback in this situation. It was decided that the primary goal of the classical design should be to make the open loop gain of the system at 400 Hz as high as practicable while still providing for a stable closed loop system. This frequency was selected because 400 Hz is the first harmonic of the highest frequency in the operating band. This will ensure that open loop gain is available at the first harmonic of all frequencies in the operating band. A secondary goal of the classical design is to provide a reasonably flat closed loop frequency response in the 26 - 200 Hz operating range. This is done by either cancelling or removing all the closed loop poles and zeros from the operating range, and ensuring that there are an equal number of closed loop poles and zeros below the operating range.

As discussed in Section 4.3, the compensation will be designed in the s-domain and converted to the z-domain for digital implementation in the controller. From the derivation in Section 4.2, the shaker transfer function $G(s)$ is given by:

$$G(s) = \frac{\ddot{X}(s)}{V(s)} = \frac{B\ell s^2}{MLs^3 + (MR + CL)s^2 + (CR + KL + B\ell^2)s + KR} \tag{27}$$

The overall plant transfer includes the system gains as well as the controller delay and is given by:

$$G_0(s) = K_1 \, e^{-sT} \, G(s) \tag{28}$$

where K_1 is the system gain and T is the controller delay. The shaker parameters $B\ell$, M, C, K, L, and R have been taken from Reference (1). The system inductance L has been revised upward from 4.27 mH to 6.5 mH to provide a better fit between the model's frequency response and the measured frequency response. This was necessary because the transfer function described by Equation (27) does not model the mutual inductances between the coils. The modeled and measured plant frequency responses are shown in Figure 5.10. The controller delay T that provides the best phase fit is 0.00045 seconds; this corresponds to a four sample delay at the 10 kHz sampling rate and a 0.5 sample delay from the ZOH.

The compensation $D(s)$ will be either a lead or lag compensator which has form

$$D(s) = K \, \frac{Qs + 1}{\alpha Qs + 1} \tag{29}$$

as discussed in Section 4.2. The parameters of this design - K, Q and α - were selected to produce the most open loop gain at 400 Hz while still maintaining a stable closed loop system. The parameters were found by a MATLAB program that iterated through the possible values of all the

parameters until the optimal set was found: $K = 1.0$, $Q = 0.00278$, $\alpha = 0.40$. Because $\alpha < 1$, this is a lead compensator design. This system is neutrally stable. To provide stability margin, K was decreased to 0.8. A bilinear transform was used to convert this compensation to the z-domain:

$$D(z) = \frac{1.9484 - 1.8796\ z^{-1}}{1.0 - 0.9140\ z^{-1}} \tag{30}$$

The frequency response $D(e^{j\omega T})$ of this compensation is shown in Figure 5.11; it is essentially an exact fit to $D(j\omega)$.

Unlike the direct digital compensation, this compensation adds gain at high frequencies, but does not add much gain at the lower frequencies (< 100 Hz). Therefore, one would expect this design to have better distortion performance at higher frequencies in the operating band, but worse performance at lower operating frequencies.

The measured and predicted open loop responses of the compensated system, $D(s)\ G_0(s)$, are shown in Figure 5.12. This figure clearly shows that the open loop gain of the system has been increased at higher frequencies; the 0 dB crossing has been extended from about 200 Hz in the direct digital design to about 600 Hz in this design. The reason the phase curves do not match is because the plant has been modeled for 4.5 sample delay and only 3.5 sample delay occurred during this particular test.

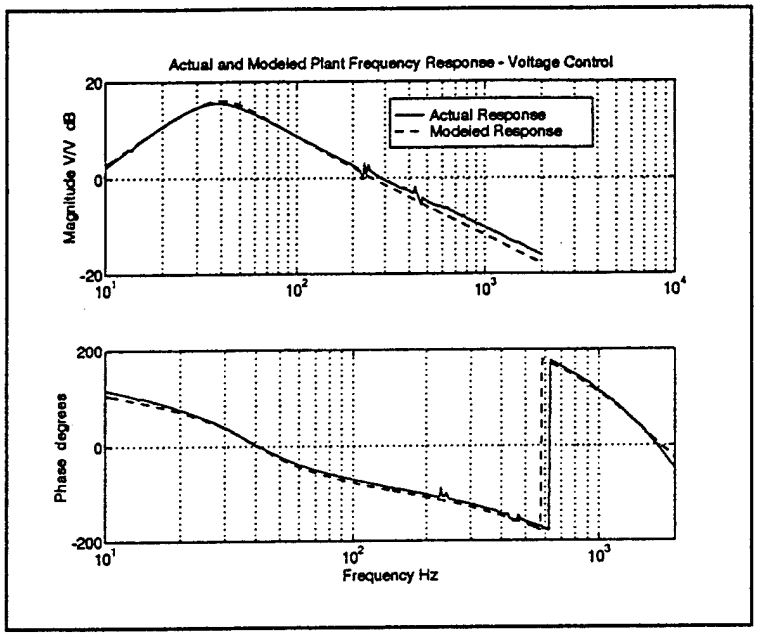

Figure 5.10

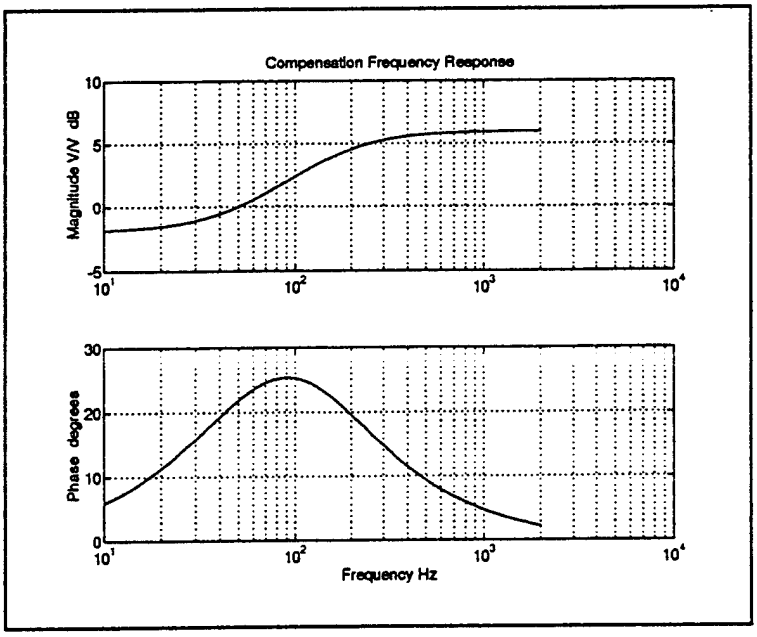

Figure 5.11

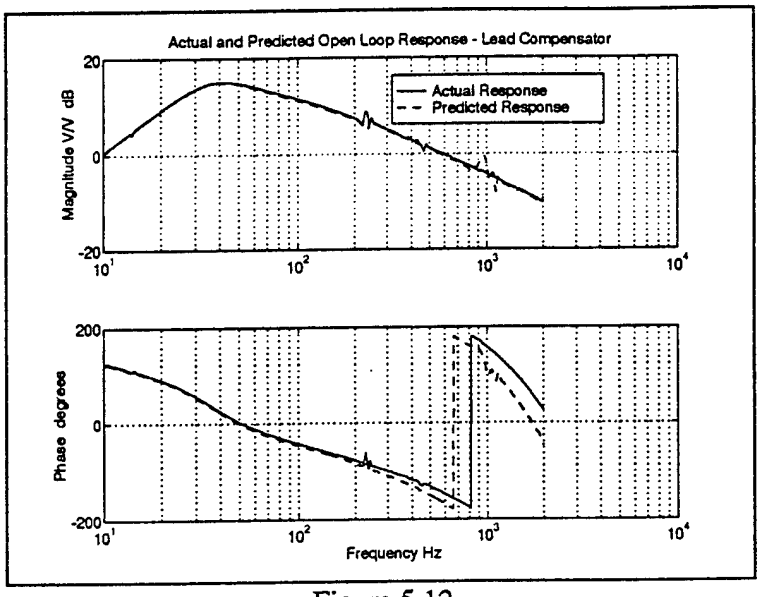

Figure 5.12

It is desired that the closed loop frequency magnitude be flat in the operating range. The degree of "flatness" will be dependent upon the closed loop poles and zeros. Figure 5.13 shows the root locus of the poles of the compensated system as well as the system minimum phase zeros; three non-minimum phase zeros are not shown. This figure shows the root locus for open loop gains ranging from 0 to 3; an "X" marks the pole locations corresponding to $K = 0.8$, the gain used for the actual compensation. For the $K = 0.8$ design, there are three poles and three zeros which effectively cancel one another out near $z = 1.0$. Of the remaining four poles, only two have an effect on the frequency response, the poles at approximately $z = 0.90 \pm 0.35j$. This complex pole pair corresponds to a natural frequency of 593 Hz with damping of 10 percent. The remaining four zeros, three non-minimum phase zeros and a zero at $z = -1.0$, have no effect on the frequency response magnitude at frequencies below 1000 Hz. Because there are no active system dynamics until the 593 Hz pole, closed loop response can be expected to be flat at frequencies below this pole. The actual and predicted closed-loop responses are shown in Figure 5.14. The differences between the actual and predicted responses are again assumed to be caused by the one sample difference between the modeled and actual controller delay. The reason that there is some small slope in the magnitude between 10 and 200 Hz is because the low frequency poles and zeros do not exactly cancel one another.

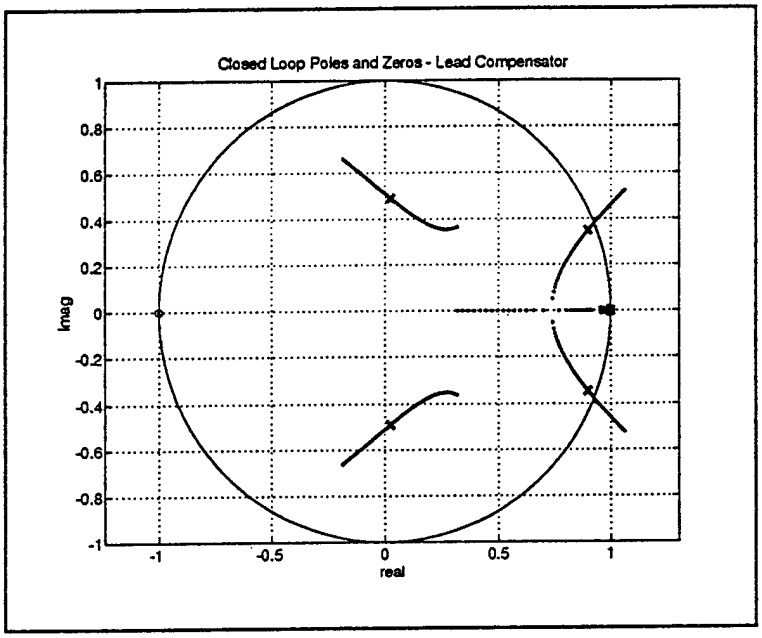

Figure 5.13

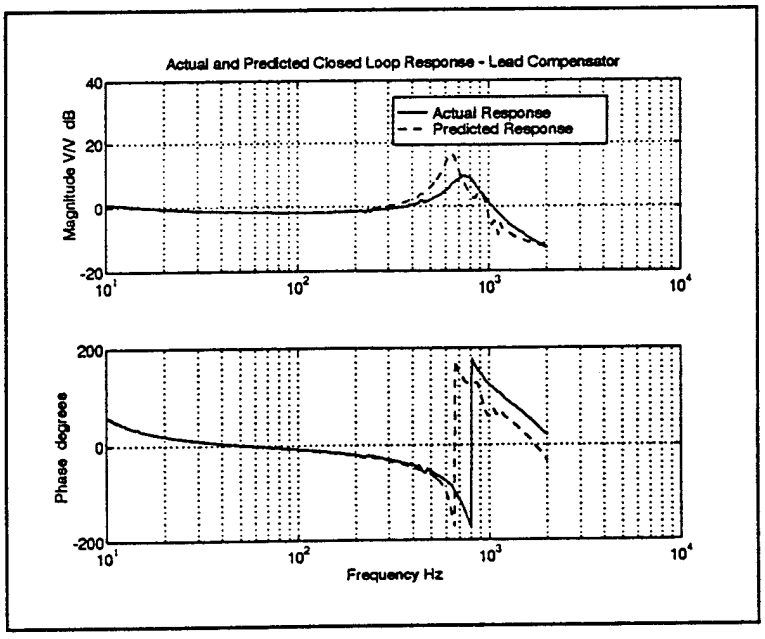

Figure 5.14

5.3 State Space Compensation Design

The state space compensation design method places the system poles with the controller gain vector $\underline{K}$ and the estimator gain vector $\underline{L}$. For purposes of comparison with the classical design approach, it was decided to place the controller poles at the same location as the closed loop lead compensator poles discussed in the last section. The estimator poles will be placed further out in the frequency range so as not to interfere with the frequency response below 1000 Hz. As discussed in Section 4.3, the compensation will work on the error signal $e[k] = v[k] - y[k]$ and will therefore be in the feedforward path. This requires that the gain vector $\underline{M}$ be set equal to $-\underline{L}$; this gain vector acts on the source voltage $v[k]$.

The desired poles from the lead compensator design are: $z = 0.0242 \pm 0.4904j$, $0.8979 \pm 0.0035j$, $0.9977 \pm 0.0035j$, 0.9683. The controller poles are placed at this location by determining the row vector $\underline{K}$ that causes the eigenvalues of $\underline{\Phi} - \underline{\Gamma}\underline{K}$ to be equal to the desired poles. $\underline{K}$ was found to be: $\underline{K} = [0.0006 \quad -0.1018 \quad -0.0048 \quad 0.2158 \quad -0.4747 \quad 1.2515 \quad -1.8381]$.

Placement of the estimator poles requires definition of the output equation matrix $\underline{H}$. It will be assumed that the output state $y[k]$ will be the plant acceleration x_1; therefore, $\underline{H} = [K_{acc}\ 0\ 0\ 0\ 0\ 0]$, where K_{acc} is the accelerometer gain of 0.2 V/g. The estimator poles will be placed such that they do not affect the plant dynamics below 1000 Hz. The desired estimator poles have been chosen to be: $z = 0, 0, 0, 0, 0, 0.3898 \pm 0.4626j$. The estimator poles are placed at these locations by determining the column vector $\underline{L}$ that causes the eigenvalues of $\underline{\Phi} - \underline{L}\,\underline{H}$ to be equal to the desired poles. $\underline{L}$ was found to be: $L = [2.0909 \quad -19.2614 \quad 401.532 \quad 0.002 \quad 0 \quad 0 \quad 0]^T$.

A comparison between the predicted closed loop systems with lead compensation and state space compensation is shown in Figure 5.15. The closed loop responses are close; the major

difference is that the state space system has greater decreasing phase at higher frequencies because of the action of the additional estimator poles.

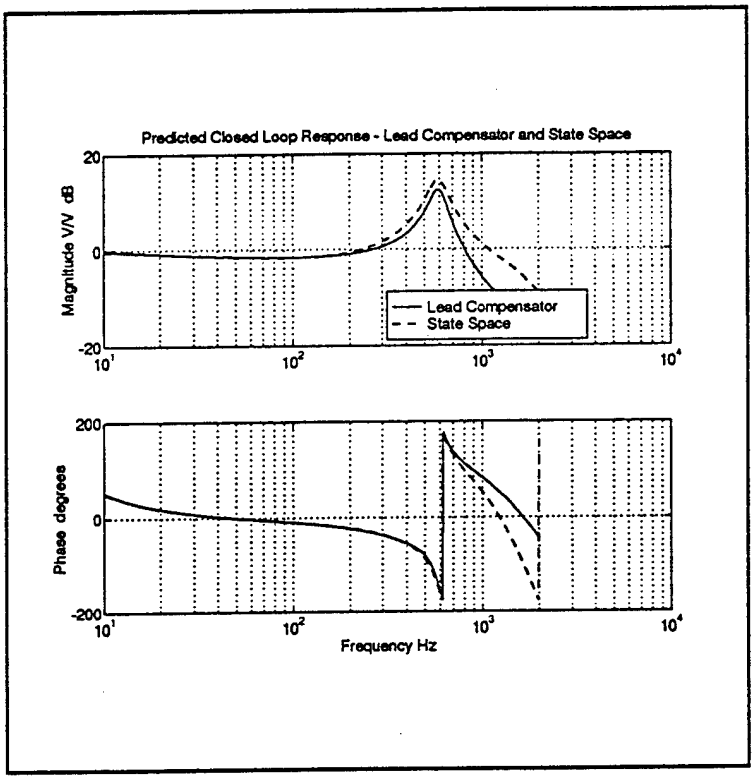

Figure 5.15

Because of lack of time and funding, it was not possible to implement the state space design method in the controller. It is anticipated that the predicted and actual responses would have matched well. Also, if sufficient time and funding existed, state space compensation would have been designed and implemented that used current feedback instead of acceleration feedback. Current feedback may be more advantageous than acceleration feedback because acceleration feedback requires an accelerometer, which may not always be available in the field.

5.4 Comments on Implementation of the Compensation

The digital compensation $D(z)$ using the direct digital and classical design methods is an IIR filter. This filter was prepared as a separate C-code function. At each interrupt, the processor would execute this function. The digital compensation function was linked with the low-level C-code that manages the communication protocols and initialization of system boards to form one executable program that operated the controller.

The IIR filter compensation was implemented as a cascade of biquad (2^{nd} order) filters. This was done to improve the numerical accuracy of the filters. A biquad filter implements the following transfer function:

$$\frac{Y(z)}{X(z)} = \frac{b_0 + b_1 z^{-1} + b_2 z^{-2}}{1 + a_1 z^{-1} + a_2 z^{-2}} \tag{31}$$

In the time domain, the output $y[n]$ of the filter is given by:

$$y[n] = b_o x[n] + b_1 x[n-1] + b_2 x[n-2] - a_1 y[n-1] - a_2 y[n-2] \tag{32}$$

This filter was implemented in the canonical form shown in Figure 5.16. This form requires that only two intermediate values, $w[n-1]$ and $w[n-2]$, be stored in system memory in order to perform the Equation (32) calculation.

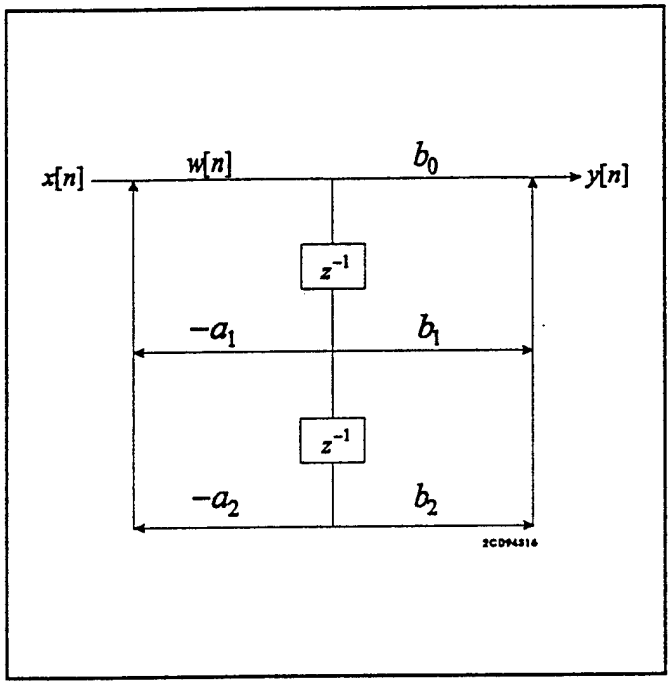

Figure 5.16

Another implementation concern was DC components in the input signals. The accelerometer could not be powered by the ICP amplifier in the analyzer because the amplifier would over range the 4.5 V input A/D. Instead, a separate impedance coupler had to power the accelerometer; this coupler prevented the power signal to the accelerometer from corrupting the accelerometer signal to the A/D.

For some of the compensation designs, even small DC components could not be tolerated. Removal of the unwanted DC component was implemented digitally with a moving-average filter. This filter is given in the time domain by:

$$r[n] = r[n-1] + \frac{1}{N}\,[x[n] - x[n-N]] \tag{33}$$

where N is the number of samples in the average. The moving average $r[n]$ was simply subtracted from the digital output signal to the D/A to prevent the output signal from containing a DC component.

Another concern was noise in the controller. It was determined that the lower 4 bits of the 16-bit A/D's were noisy. The only effective method of removing this noise was to zero these bits, leaving only 12-bit A/D's. Testing was not conclusive as to whether zeroing these bits improved performance.

6. DISTORTION TESTING

A major goal of the digital controller is to reduce the total harmonic distortion of the shaker. This section presents the results of the distortion testing of the shaker with and without digital feedback compensation.

Figure 6.1 shows the baseline total harmonic distortion (THD) of the shaker with the amplifier in voltage control. Three curves are presented in this figure representing the THD at 50, 5.0, and 0.5 lbf at all frequencies in the 26 - 200 Hz operating band. Figure 6.2 shows the same baseline THD measurements but with the amplifier in current control. The results show that the distortion for the most part is below one percent in the operating band. Some notable exceptions to this are the voltage controlled, low frequency 50 lbf distortion and the voltage controlled, high frequency, 0.5 lbf distortion. The reason for the increased low frequency distortion at 50 lbf is the nonlinearity of the

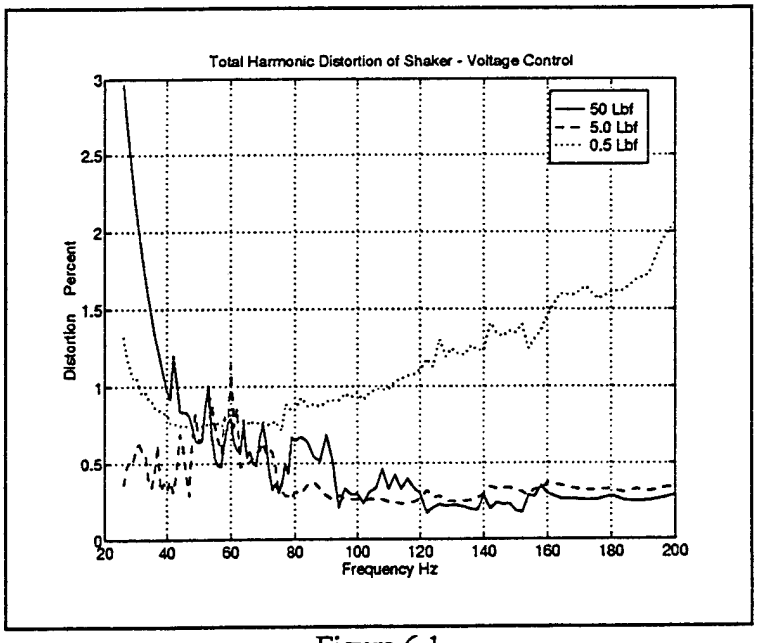

Figure 6.1

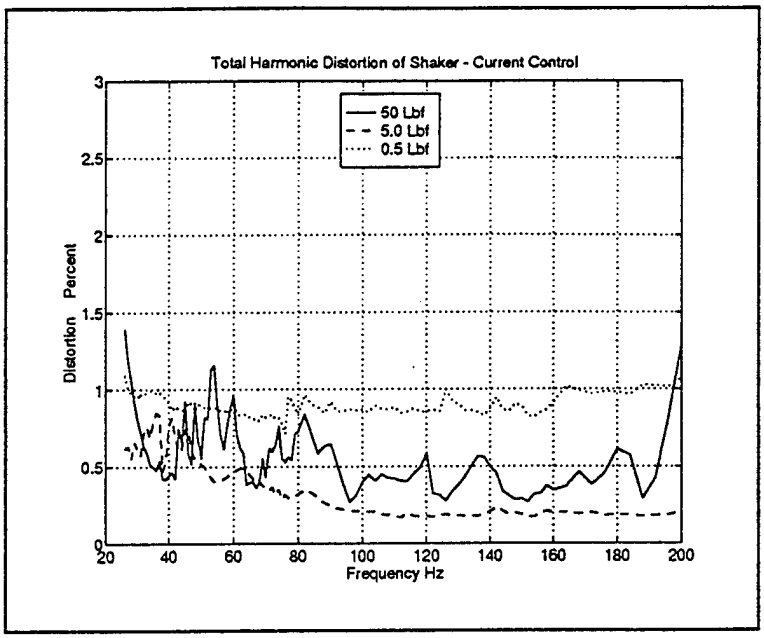

Figure 6.2

magnetic field. The reason for the increased high frequency distortion at 0.5 lbf is stiction. In the voltage controlled tests, the force output corresponds to the force output at 26 Hz. At higher frequencies, the force decreases because of the increased electrical impedance of the shaker. In fact, the 0.5 lbf level drops to about 0.3 lbf at 200 Hz. The increased stiction is due to the lower force level. Other than in those two areas, the current controlled and voltage controlled measurements are similar.

Figures 6.3 and 6.4 show the THD with the direct digital feedback compensation and the amplifier in voltage control and current control, respectively. Because the transfer function magnitude is essentially 0 dB across the frequency range with feedback compensation, the force level remains essentially constant during the feedback tests. These results show that, in general, the low frequency distortion has been decreased with feedback and the high frequency distortion has either remained the same or increased. This is best shown by Figures 6.5 and 6.6, which are plots of the change in THD when feedback is introduced; a positive change indicates an increase in distortion with feedback, a negative change indicates a decrease in distortion with feedback. The distortion reduction with feedback is greatest at the higher force levels. This is believed to be because the noise in the

controller reduces the performance at low force levels. The reason for the increased distortion with feedback is considered to be primarily caused by the controller noise; some aliasing of high frequency controller noise may also be occurring.

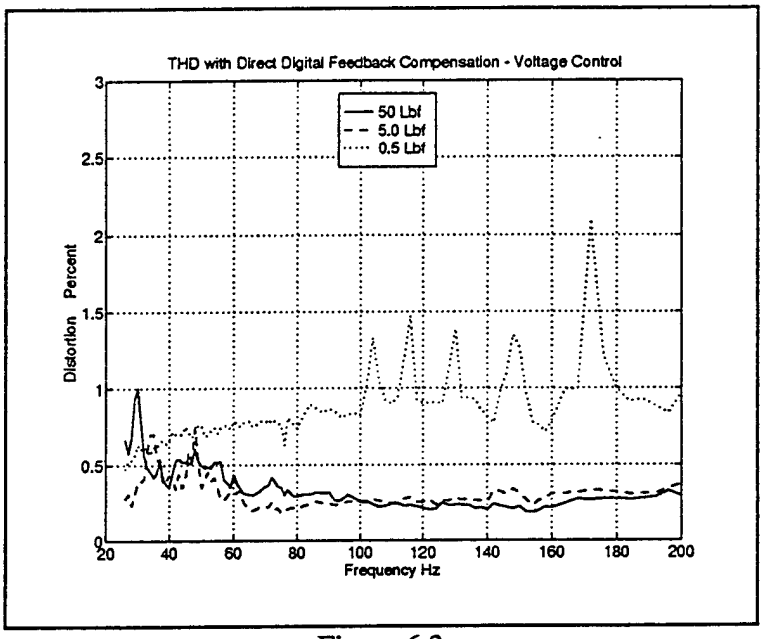

Figure 6.3

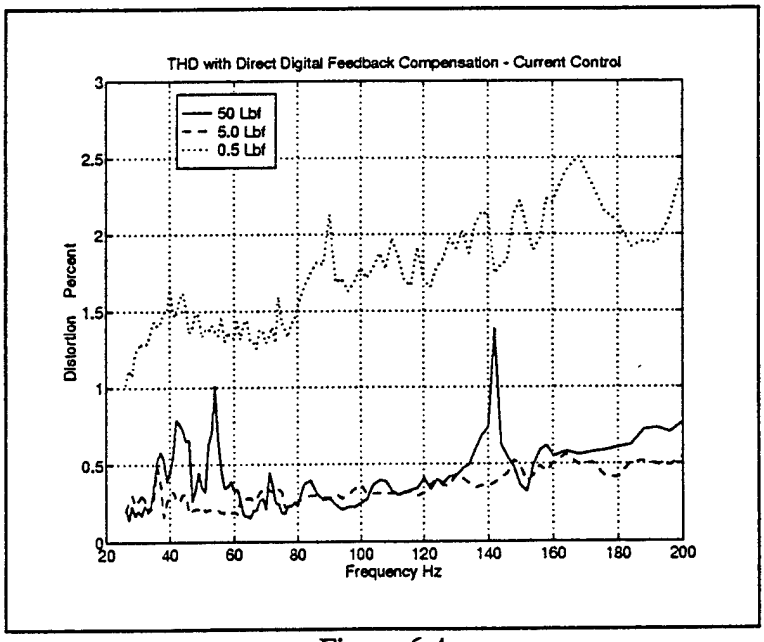

Figure 6.4

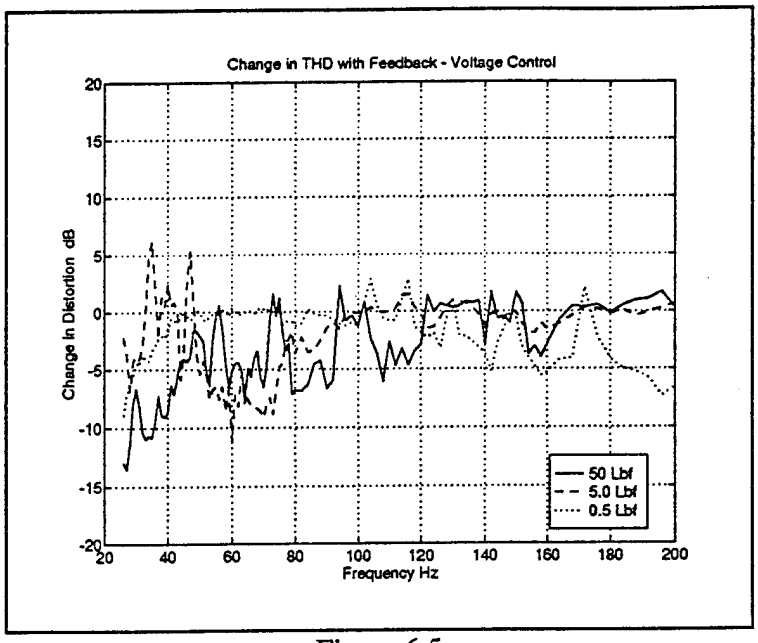

Figure 6.5

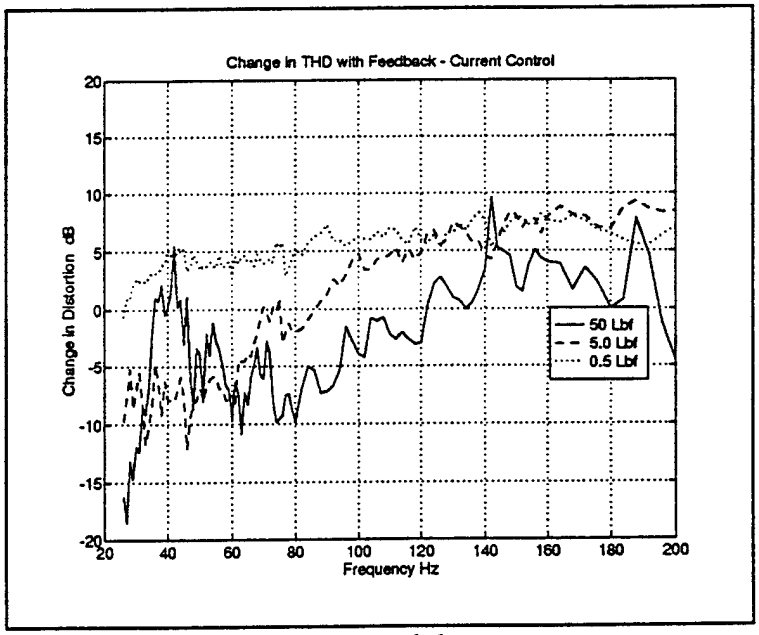

Figure 6.6

The reason for the better performance at low frequencies is most attributable to the increased open loop gain at the drive frequency harmonics. Figure 6.7 compares the open loop gain at the first harmonic (two times the fundamental frequency) with the change in distortion with feedback at that harmonic. For example, the curve values at 26 Hz correspond to the open loop gain at 52 Hz and the change in the first harmonic distortion at 52 Hz. This curve indicates the dependence between open loop gain and distortion; the first harmonic distortion for the 50 lb drive level appears to be almost a reflection of the open loop gain.

The THD with lead compensation feedback is shown in Figure 6.8; Figure 6.9 shows the change in first harmonic distortion versus open loop gain for the lead compensator. These curves exhibit the same characteristics as the distortion curves with the direct digital compensation. It was anticipated that there would be greater reduction in the high frequency distortion because of the increased open loop gain of the lead compensator, but this effect is not observed.

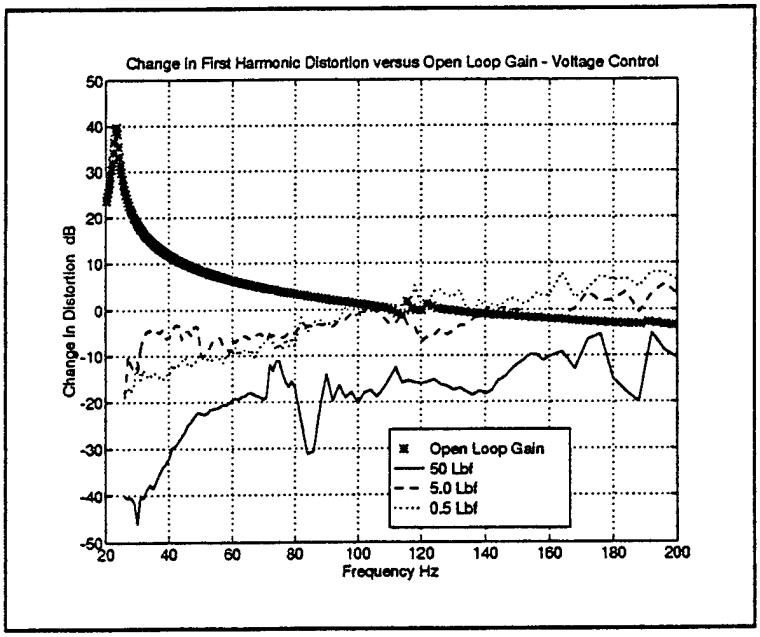

Figure 6.7

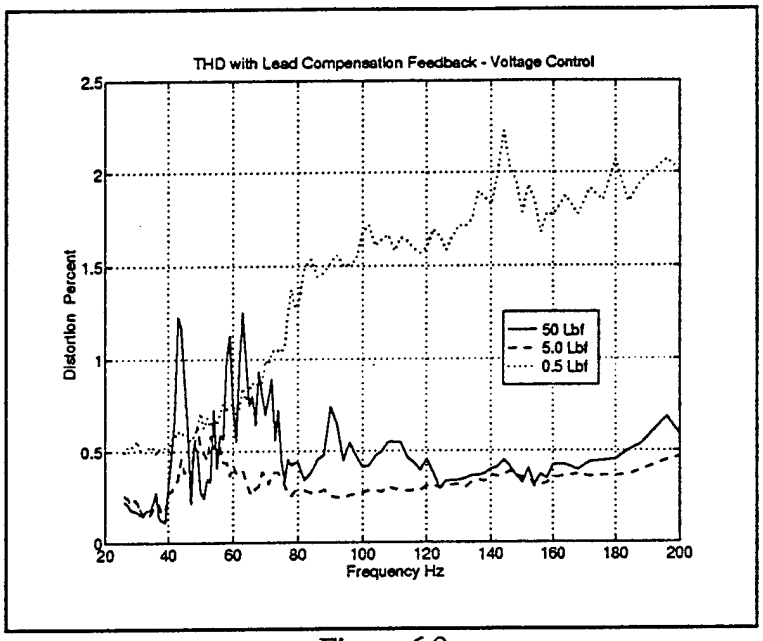

Figure 6.8

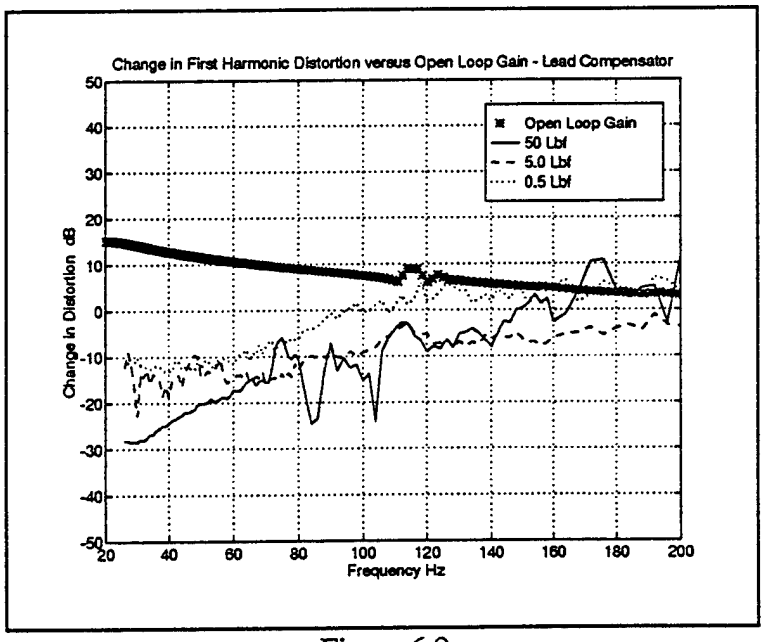

Figure 6.9

This distortion testing clearly shows that a reduction in total harmonic distortion is obtained with feedback, and the amount of distortion reduction is dependent upon the open loop gain at the harmonics. The direct digital compensation seems to provide slightly more distortion reduction than the lead compensator, primarily because of the direct digital compensation's large open loop gains at the lower frequencies. At the higher operating frequencies, some increase in distortion with feedback sometimes occurs. This can be attributed to noise in the controller and the decrease in open loop gain at the higher frequencies.

7. DIGITAL CONTROLLER AUTOMATED DESIGN TECHNIQUE AND SOFTWARE

The direct digital compensation design process can be automated so that the controller develops the desired compensation "on-line" without human intervention. C-code for doing this has been written, compiled, and downloaded onto the digital signal processing (DSP) board. Simulations of the automation process have been performed on models of the shaker transfer function with C-code executables on a personal computer. The simulations have been successful. Similar simulations have been performed using the digital signal processing board. These simulations have not been completely successful because the curve fitting function has been unable to accurately fit the plant transfer function with the single precision arithmetic of the digital signal processing board. Improvements in the curve fitting function have been developed which should correct this problem; however, these improvements have not been implemented in C-code and run on the digital signal processing board because of time constraints. Nevertheless, the automation process appears achievable, and more than 90 percent of the C-code to implement it in real-time in the controller has been prepared. This section discussed the automation algorithm and its implementation.

The automation algorithm basically implements the direct digital compensation method discussed in Sections 4.1 and 5.1. A flow chart for the algorithm is shown in Figure 7.1. Each block of the diagram has been implemented by a separate C-code function. A brief description of each of the blocks follows:

- Global Parameters Block - This function sets the parameters of the design process, such as sampling rate, desired Butterworth filter breakpoints, maximum open loop gain, accelerometer gain, system identification bandwidth, etc. The function is setup with default values for the parameters and the user selects which, if any, parameters to change. The C-compiler that comes with the digital signal processing board does not recognize the ANSI Standard scanf ( ), getc ( ) functions, and is therefore not able to accept input data from a

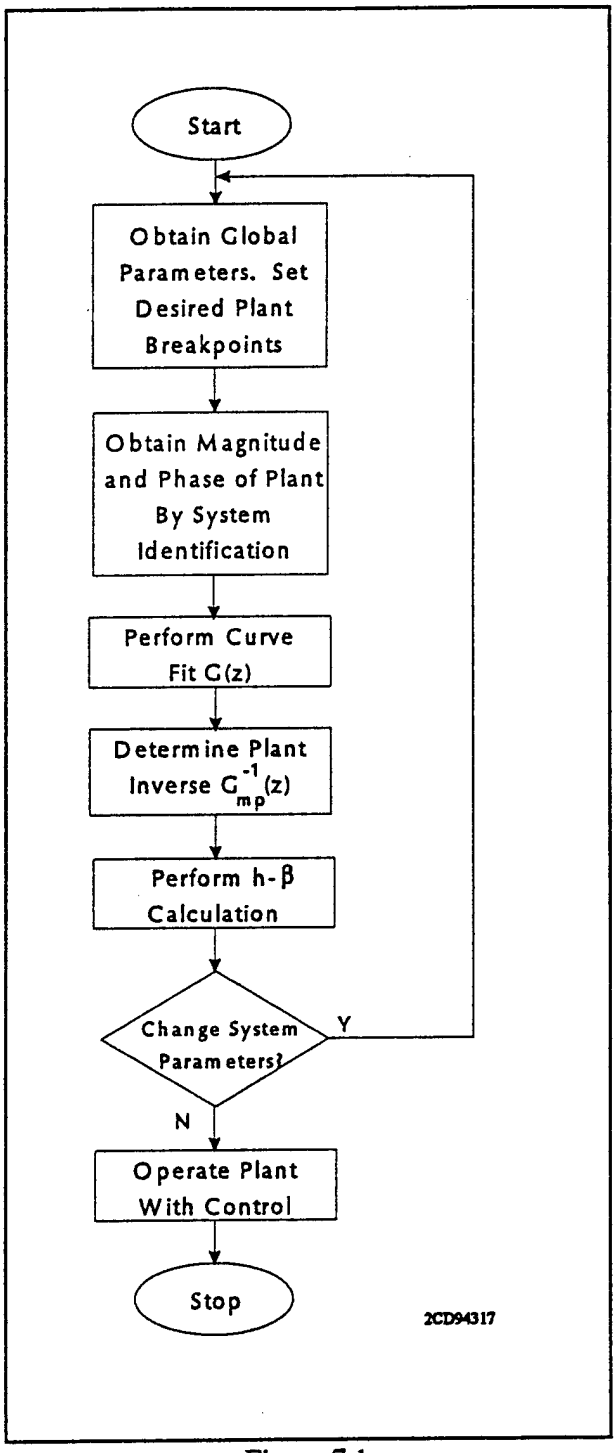
Start
Obtain Global Parameters. Set Desired Plant Breakpoints
Obtain Magnitude and Phase of Plant By System Identification
Perform Curve Fit G(z)
Determine Plant Inverse $G_{mp}^{-1}(z)$
Perform h-β Calculation
Change System Parameters?
Y
N
Operate Plant With Control
Stop
2CD94317

Figure 7.1

keyboard. Because of this, the parameter values have to be set in the source C-code. Any changes to the parameters must be made in the source C-code and the code recompiled. It is expected that functions can be prepared that will allow data input from a keyboard in the future.

- System Identification Block - This block performs either a swept sin or a tone burst identification of the plant. The duration and bandwidth of the tone burst is set by the user; the system identification is obtained by dividing the fast Fourier transform (FFT) of the output by the FFT of the tone burst. Because of the use of an FFT algorithm, the sample rate must be a power of two. The swept sin identification uses a digitally generated sin wave as the plant input and performs a discrete Fourier transform (DFT) on the output signal. A DFT is used because only the content of the drive frequency bin is determined. The algorithm requires that the sample rate be a factor of two.

- Curve-Fit Block - This function fits the system identification phase and magnitude information to an IIR filter. The user specifies the maximum number of poles and zeros required for the curve fit. The function starts by fitting the plant to one pole and one zero, calculates the average error between the plant and the fit, increments the number of poles and zeros by one, and continues the process until the maximum number of poles and zeros have been reached. It then selects the IIR filter with the least error. The curve fitting routine used is similar to the invfreqz function in MATLAB.

- Plant Inverse Block - This function removes the non-minimum phase zeros from the IIR filter $G(z)$ and then inverts the filter. The non-minimum phase zeros are determined by finding the magnitude of the roots of the numerator of $G(z)$. After removing the non-minimum phase roots, and the gain of the plant adjusted to be the same as before, the fit between the magnitude of the modified filter and the plant is checked to ensure that the fit is

still good. The non-minimum phase zeros are then convolved into the desired Butterworth bandpass filter to produce the modified desired plant.

- h - β Block - This function determines the feedback gain h and the compensation $\beta(z)$ in accordance with Equation (4). The compensation $\beta(z)$ is determined for consecutively larger values of the feedback gain h until the maximum allowable, user-set feedback gain is reached or the filter $\beta(z)$ becomes unstable.

- Control System Operation Block - This block implements the compensation $\beta(z)\ G_{mp}^{-1}(z)$ in the real-time control system. At present, this function is written as one large IIR filter in canonical form. For reasons of numerical accuracy, it may be necessary to implement this filter as a cascaded set of biquad filters.

8. CONCLUSION

The goal of the Radix Systems, Inc. 50 lbf moving magnet actuator digital controller was to flatten the actuator's frequency response magnitude and reduce THD in the 26-200 Hz operating band; the controller has satisfactorily met both these goals. The frequency response magnitude of the shaker without compensation varies from 3 to 16 dB in the operating range; with closed loop control the magnitude is within ± 1 dB in the operating range. In general, the THD has decreased an average of 5 to 10 dB over the operating range with feedback. The level of the first harmonic was shown to decrease as much as -20 to -40 dB in areas of high open loop gain. The amount of open loop gain was found to be directly related to the amount of THD.

Digital feedback compensation was developed using direct digital, classical, and state space methods. Each of the methods developed satisfactory compensation, although the direct digital appears the most appropriate for the design goals. The classically designed compensation is the easiest to implement and the most fundamental. The state space design approach introduced the idea of providing current feedback instead of acceleration feedback if the acceleration state is not available.

Finally, a technique was described for automating the entire digital compensation design process. This process allows the controller to determine the required digital compensation for the application without human intervention. Several simulations were run on models - including a model of the shaker - that showed that the automated process developed correct compensation.

The digital controller described in this report is far from perfect. It contains a delay that varies between 3.5 and 4.5 samples; it is only able to sample up to 30 kHz; it generates system noise. These problems limit the shaker bandwidth and increase distortion. Despite these problems, the controller was still able to improve the overall performance of the shaker. With further work on the hardware

and low-level software of the controller, it is expected that these problems could be greatly minimized and the overall shaker performance enhanced.

9. REFERENCES

(1) "Design Report and Test Results for Radix Systems, Inc. 50 Lb Convective Moving Magnet Actuator," Radix Systems Report No. TR-94-087, May 1994.

(2) "Design Methodology for Moving Magnet Actuator and Application to 50 Lb Prototype," Radix Systems Report No. TR-93-079, January 1993.

(3) "Detailed Design and Preliminary Test Report for 50 Lb Prototype Moving Magnet Actuator," Radix Systems Report No. TR-93-084, August 1993.

(4) "Final Test Results for 50 Lb Prototype Moving Magnet Actuator and Application to 500 Lb Actuator Design," Radix Systems Report No. TR-94-085, November 1993.